nature chemical biology

Article

https://doi.org/10.1038/s41589-024-01628-y

Transcriptional regulation of living materials via extracellular electron transfer

Received: 26 May 2023

Accepted: 19 April 2024

Published online: 23 May 2024

Check for updates

Austin J. Graham[1,4], Gina Partipilo[1,4], Christopher M. Dundas[1], Ismar E. Miniel Mahfoud[2], Kathleen N. Halwachs[1], Alexis J. Holwerda[2], Trevor R. Simmons[1], Thomas M. FitzSimons[1], Sarah M. Coleman[1], Rebecca Rinehart[1], Darian Chiu[1], Avery E. Tyndall[3], Kenneth C. Sajbel[1], Adrianne M. Rosales[1] & Benjamin K. Keitz[1]

Engineered living materials combine the advantages of biological and synthetic systems by leveraging genetic and metabolic programming to control material-wide properties. Here, we demonstrate that extracellular electron transfer (EET), a microbial respiration process, can serve as a tunable bridge between live cell metabolism and synthetic material properties. In this system, EET flux from *Shewanella oneidensis* to a copper catalyst controls hydrogel cross-linking via two distinct chemistries to form living synthetic polymer networks. We first demonstrate that synthetic biology-inspired design rules derived from fluorescence parameterization can be applied toward EET-based regulation of polymer network mechanics. We then program transcriptional Boolean logic gates to govern EET gene expression, which enables design of computational polymer networks that mechanically respond to combinations of molecular inputs. Finally, we control fibroblast morphology using EET as a bridge for programmed material properties. Our results demonstrate how rational genetic circuit design can emulate physiological behavior in engineered living materials.

Living polymer networks, including tissues and biofilms, actively respond to complex combinations of environmental inputs leading to differentiation, regeneration and development[1]. In these systems, the bidirectional flow of chemical[2], mechanical[3,4] and electrical[5,6] information between constituent cells and their extracellular matrix informs micro- and macroscopic morphology and function. This dynamic reciprocity is made possible through distributed sensing and actuation machinery controlled by genetic regulatory networks[7,8]. Consequently, continuous feedback between gene expression and material properties controls morphology, patterning and hierarchical assembly.

Mimicking these natural processes, engineered living materials (ELMs) seek to capitalize on the programmability of living systems to control material synthesis and system-wide properties[9]. For example, *Escherichia coli* cells expressing curli fibers can be engineered to create a variety of soft materials including pressure sensing devices[10], probiotic biofilms[11] and protein-based hydrogels[12,13]. Similarly, embedding engineered cells into exogenous hydrogels results in materials with advanced sensing capabilities[14–17]. These studies provide an important conceptual foundation for living materials, but material properties are often decoupled from genetic programming. For example, many ELMs require considerable postprocessing to create the desired material function, exhibit phenotypes (that is, fluorescence) that do not interface with the material or do not fully leverage the computational and sensing capabilities of whole cells. To fully recapitulate natural materials and their advantages in many applications, future ELMs will require coupling cell growth and gene regulatory networks to changes in material properties.

[1]McKetta Department of Chemical Engineering, University of Texas at Austin, Austin, TX, USA. [2]Interdisciplinary Life Sciences Graduate Program, University of Texas at Austin, Austin, TX, USA. [3]Department of Chemical and Biological Engineering, Colorado School of Mines, Golden, CO, USA. [4]These authors contributed equally: Austin J. Graham, Gina Partipilo. e-mail: keitz@utexas.edu

https://doi.org/10.1038/s41589-024-01628-y

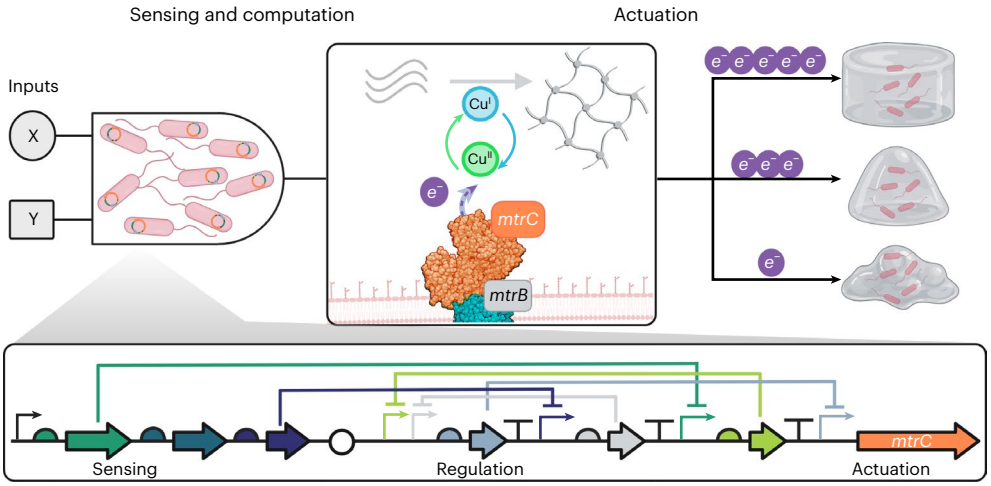

Fig. 1 | Bacterial sensing and computation actuate material mechanics. Schematic illustrating computational polymer networks actuated by transcriptional logic. *S. oneidensis* acts as a distributed computing element within a network precursor solution, and input signals activate (or deactivate) expression of an EET-pathway protein (MtrC). When placed under transcriptional regulation, MtrC generates different amounts of EET flux and controls the redox state of a catalytic metal. On reduction, the metal catalyst powers a chemical reaction such as ATRP or CuAAC. This results in a living synthetic polymer network whose mechanical properties are coupled to biological computation. Created with Biorender.com.

Many ELMs leverage the properties of synthetic polymer networks, which are more chemically, mechanically and functionally diverse[18,19] relative to biologically derived materials. However, they generally lack mechanisms for advanced sensing, computation and actuation because it is challenging to interface biological programming with material properties. Efforts to program abiotic polymer networks with biomimetic behavior have seen some success[20–23], but purely chemical approaches typically require large input signals and multiple orthogonal chemistries, limiting their programmability to relatively simple operations[24–26]. Thus, marrying the functional advantages of synthetic materials with the ability of cells to programmability sense, compute and actuate material changes could yield advanced materials germane to several fields, including tissue engineering[9], additive manufacturing[27] and autonomous materials[28]. To address this challenge, we propose utilizing microbial EET[29], a respiratory mechanism in electroactive microbes that couples metal oxidation state to central carbon metabolism, as a means to control polymer network cross-linking via biological reduction of metal catalysts[30,31].

Here we describe synthetic polymer networks (that is, hydrogels) that cross-link in response to multi-input logic computations performed by embedded bacteria (Fig. 1). Leveraging transcriptional control over key EET genes in the model electrogen *Shewanella oneidensis* (wild-type strain, MR-1), we deploy engineered bacteria as distributed computing and actuating elements within a solution-phase network precursor. On sensing dilute chemical stimuli, *S. oneidensis* strains transcriptionally regulate EET protein expression, which subsequently reduces and activates the metal catalysts responsible for network cross-linking. First, we show that atom-transfer radical polymerization (ATRP) cross-linking can be dynamically coupled to gene expression to predictably control polymer network mechanics through single-input transcriptional regulation. From these, we develop design guidelines using approaches from synthetic biology that inform forward engineering of living material mechanics. We then expand the logical complexity of our polymer networks by engineering two-input genetic Boolean circuits (OR, NOR, AND and NAND) for controlling EET protein expression and resultant gel mechanics. Capitalizing on the ability of EET to interface with diverse metal–ligand pairs, we also demonstrate that identical transcriptional logic can control another well-known cross-linking chemistry, copper(I)-catalyzed alkyne-azide cycloaddition (CuAAC). Finally, we apply this technology as an ELM-tissue engineering interface to control the morphology of fibroblasts seeded onto hydrogels formed via bacterial logic-driven regulation over EET. By coupling whole-cell biological computation to the activity of synthetic cross-linking catalysts, we showcase EET's potential as a universal interface for programming polymer network properties and forward engineering living materials using genetic circuits.

Results

Relative gene expression correlates with material mechanics

We initially hypothesized that on-demand polymer network synthesis could be programmed using stimuli-responsive genetic circuits controlling EET gene expression. For example, we previously demonstrated that a transcriptional circuit regulating a single EET gene, *mtrC*, in *S. oneidensis* could predictably control the mechanical properties of cross-linked hydrogels formed via radical polymerization[31]. In this system, EET to a redox-active copper catalyst controlled the cross-linking rate and hydrogel stiffness (measured as storage modulus, G') of methacrylated bio-macromers through ATRP[31]. However, a major limitation of this previous strategy was a requirement to separate EET gene expression from cross-linking. This was achieved by growing bacteria anaerobically to stationary phase, then inoculating induced cells into macromer solutions. This strategy ensured that bacterial respiration was completely anaerobic and that the transcriptionally controlled EET genes had established steady-state protein levels before mixing with polymerization components (Fig. 2a). However, this temporal separation of gene expression, protein maturation and chemical cross-linking does not mimic natural systems, in which sensing, growth and actuation are integrated. Ideally, ELMs should autonomously sense environmental signals, regulate the expression of an appropriate gene and actuate material transformations in real-time. We therefore sought to couple cell metabolism and gene expression to cross-linking, such that hydrogels would form dynamically in response to naïve *S. oneidensis* cells detecting appropriate stimuli.

To examine this possibility, we inoculated an uninduced, EET-deficient knockout (Δ*mtrC*Δ*omcA*Δ*mtrF*) complemented with *mtrC* under the control of the LacI–$P_{tacsymO}$ regulator–promoter pair into an aerobic gel precursor mixture. This strain was grown under aerobic conditions to inhibit native EET protein expression[32], and therefore lacked upstream EET-pathway components as well as transcriptionally regulated *mtrC* on inoculation into the precursor mixture. The gel

https://doi.org/10.1038/s41589-024-01628-y

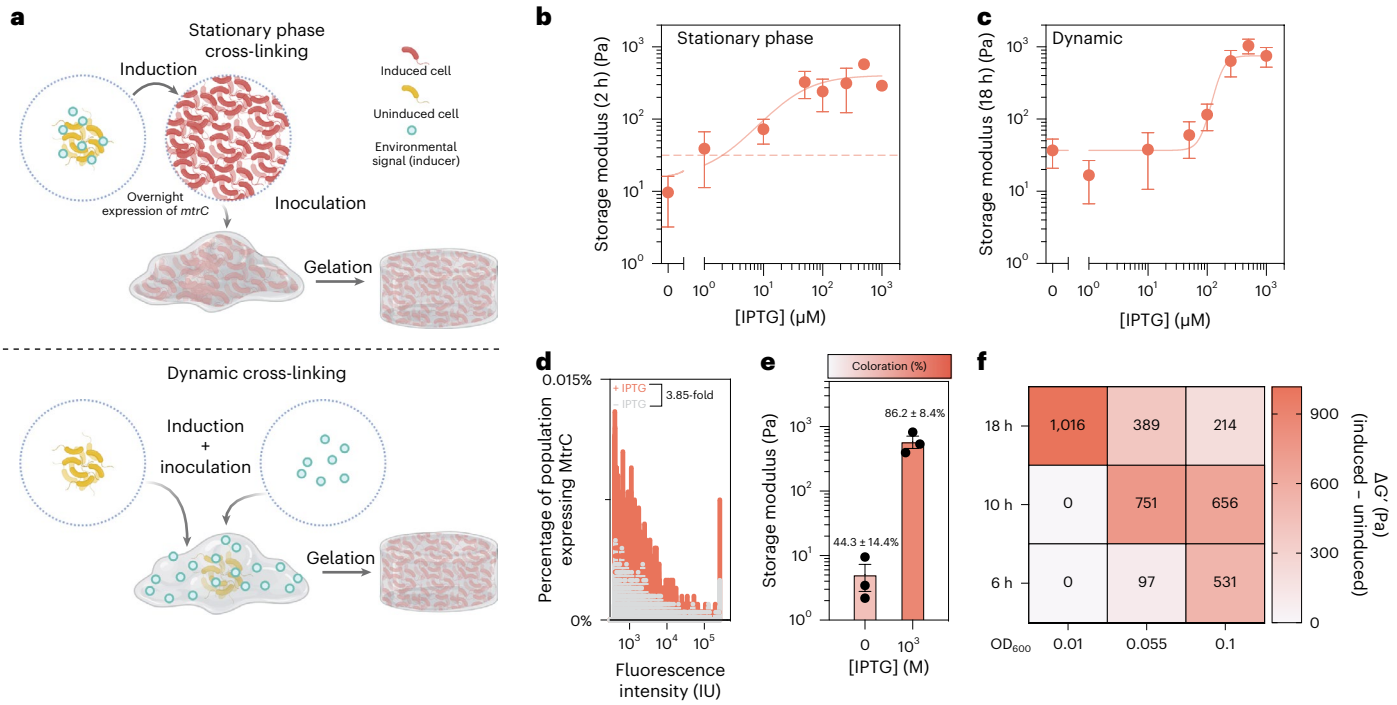

Fig. 2 | Transcriptional control of EET proteins enables dynamic cross-linking tunable by inoculation density, inducer concentration and reaction time. **a**, Schematic illustrating stationary phase versus dynamic cross-linking. Under dynamic cross-linking conditions, naïve cells are only exposed to the inducer following inoculation into the pregelation mixture. Created with Biorender.com **b**, Gel storage modulus measured as a function of inducer concentration show characteristic transcriptional regulation under stationary phase cross-linking. The dashed line represents storage modulus of gels using induced empty vector strains. **c**, Gel storage modulus measured as a function of inducer concentration show characteristic transcriptional regulation under dynamic cross-linking. Gels did not form in the presence of corresponding knockout strains harboring an empty vector. **d**, Histogram of flow cytometry results between induction (1 mM IPTG) and basal expression (0 mM IPTG) of an MtrC mutant containing His- and StrepTagII-antibody labeled with AlexaFluor 647 under control of LacI–$P_{tacsymO}$. **e**, Storage modulus and percentage color change of gels harvested after 18 h and incubated with Fe(III) and ferrozine. Color change measured after 10 min as an indicator of reduction capability of embedded bacteria. **f**, Dynamic range of storage moduli accessible at multiple cell inoculum and reaction times under dynamic cross-linking conditions, without requiring previous expression of *mtrC* (heatmap represents $n = 1$). Data shown are mean ± s.e.m. of $n = 3$ biological replicates.

precursor solution contained a Cu catalyst (Cu-tris(2-pyridylmethyl) amine, Cu-TPMA), a radical initiator (2-hydroxyethyl 2-bromoisobutyrate, HEBIB), four-arm methacrylate-functionalized poly(ethylene glycol) polymer (PEG-methacrylate) and inducer (isopropyl-β-D-thiogalactopyranoside, IPTG). Despite the requirements for coordinated cell growth, oxygen removal and protein expression, cross-linking occurred to create hydrogels. Naive cells formed gels on induction in a dose-dependent manner (Fig. 2a,c). Fully induced, dynamic *mtrC* expression yielded stiff gels with relatively similar plateau moduli compared to steady-state *mtrC* expression (Fig. 2b,c), while uninduced basal *mtrC* expression was correlated with weaker gels (Fig. 2c). Gels did not form in dynamic cross-linking conditions when using an EET-deficient knockout harboring an empty vector control. In addition, wild-type bacteria that were allowed to incubate in the macromer mixture aerobically for 18 h could then be sealed in reaction vessels to form hydrogels on demand (Supplementary Fig. 1). This is only possible using a dynamic cross-linking system. To further validate that transcriptional regulation of *mtrC* was indeed driving dynamic cross-linking, increased protein expression on IPTG induction was independently confirmed using flow cytometry with tagged variants of MtrC (StrepTagII-MtrC-His) and quantitative PCR with reverse transcription (Fig. 2d and Supplementary Fig. 2). Additionally, expression of MtrC was indirectly measured for induced and uninduced gel systems where gels were subsequently incubated with Fe(III) and ferrozine to detect *Shewanella*-generated Fe(II) via colorimetric shift[33] (Fig. 2e). Finally, cells exhibited no growth defects in gel precursor solutions and remained viable and metabolically active for up to 1 week following encapsulation (Extended Data Fig. 1). Together, these results confirm that naïve cells, which have not previously been exposed to any stimulus, can dynamically couple *mtrC* expression to material properties.

In contrast to standard fluorescent reporters, which are typically measured under static and/or steady-state conditions, both transcriptional output (*mtrC* expression) and resulting function (network cross-linking) are dynamic processes in our system. Therefore, we examined different cross-linking reaction times to optimize ON/OFF mechanical differences between gels formed using induced and uninduced cells. The dynamic range of gel stiffness (ratio of induced to uninduced values) was robust to both changes in incubation time and initial cell density; however, the best dynamic range was observed with low initial inoculation size and long reaction times (~18 h) (Fig. 2f). Alternative EET machinery to *mtrC* (*mtrA*, *cymA*) could also be transcriptionally regulated to control network cross-linking, highlighting the programmability of EET pathways in *S. oneidensis* for material synthesis (Extended Data Fig. 2 and Supplementary Fig. 3). Ultimately, we opted to control *mtrC* expression in subsequent genetic circuits due to this construct's high dynamic range and the resultant protein being the direct actuator of catalyst reduction.

Based on our success in linking dynamic *mtrC* expression to gel cross-linking, we predicted that changes to the inducer-sensing regulator would enable material computation analogous to previously developed circuits using fluorescent reporters[34,35]. To examine this

https://doi.org/10.1038/s41589-024-01628-y

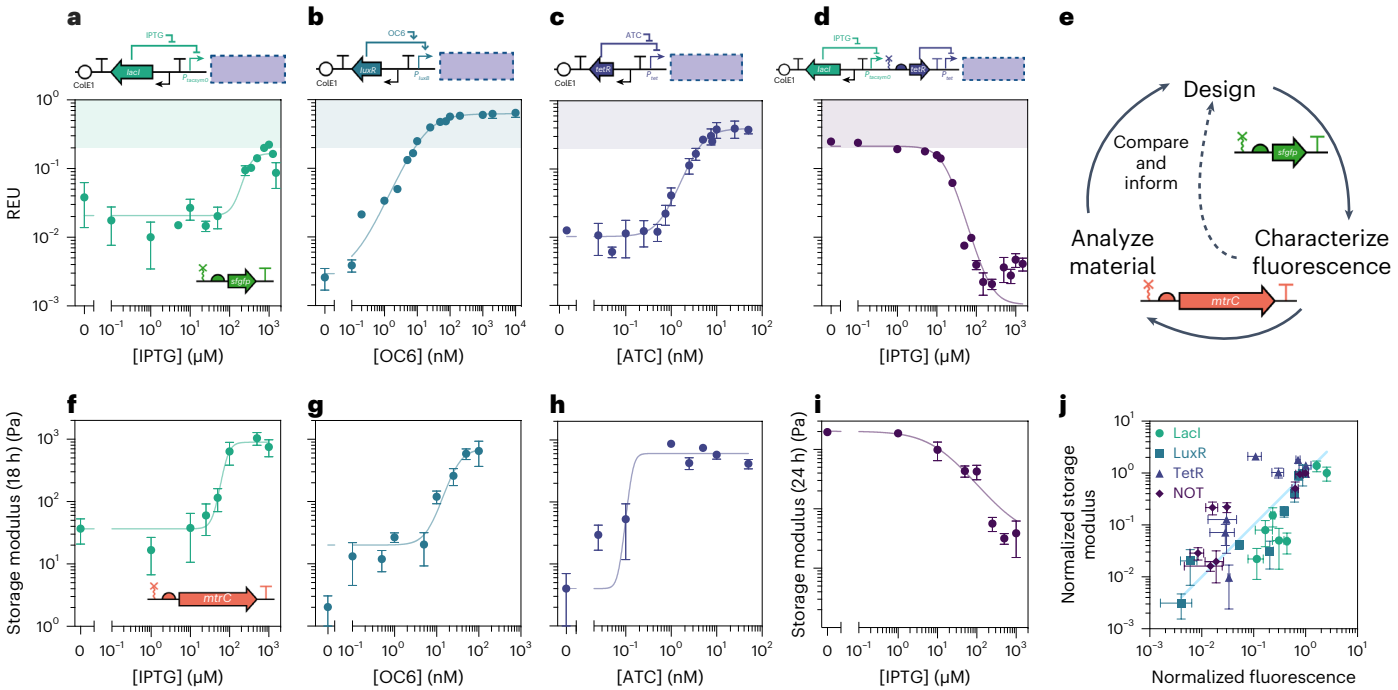

Fig. 3 | Transcriptional regulation of *mtrC* yields predictable control over polymer network mechanics via fluorescent gate parameterization. a–**c**, REU measured as a function of inducer concentration show characteristic transcriptional regulation over a variety of dynamic ranges for multiple traditional buffer gate architectures: IPTG (**a**), OC6 (**b**) and ATC (**c**). **d**, A NOT gate architecture expressing *sfgfp*. Shaded regions above REU of 0.3 indicate approximate induction levels at which inducible control over hydrogel mechanics is lost. **e**, Schematic of a feedback loop representing adaptation of fluorescent circuit parameterization for applications in living materials. Created with Biorender.com. **f**–**h**, Storage moduli of methacrylated PEG polymer networks dynamically cross-linked via expression of *mtrC* from the same circuits in **a**–**c**, measured after 18 h postinoculation: IPTG (**f**), OC6 (**g**) and ATC (**h**). **i**, A NOT gate architecture expressing *mtrC* at 24 h postinoculation. **j**, Fluorescence versus storage moduli for corresponding circuits, each normalized by their value at maximum induction (or minimum in the case of NOT gate), plotted at equivalent levels of induction to demonstrate the agreement between fluorescent characterization and material response. The line of identity ($y = x$) is drawn to demonstrate agreement with a Pearson's R value of 0.5761 and $P < 0.0007$. Data shown are mean ± s.e.m. of $n = 3$ biological replicates.

possibility, we constructed Buffer gate plasmids containing the regulator–promoter pairs LacI–$P_{tacsymO}$, LuxR–P_{Lux} and TetR–P_{Tet} to drive transcription of either *sfgfp* or *mtrC* in response to their cognate inducers (IPTG, 3-oxohexanoyl-homoserine lactone (OC6) and anhydrotetracycline hydrochloride (ATC), respectively). We parameterized circuit outputs using fluorescent reporter relative expression units (REUs), which has facilitated circuit debugging and optimization in similar transcriptional circuits that regulate RNA polymerase flux[34,36]. As REU measurements can enable forward engineering of gene expression and design of complex cellular logic, we also leveraged this metrology to probe how *mtrC* circuits affected EET-driven hydrogel formation. Using *S. oneidensis* strains transformed with *sfgfp* circuits, we initially assessed the transcriptional control of each buffer gate by measuring fluorescence after overnight growth in inducer-containing media. REU values were determined by normalizing measurements to fluorescence from an *S. oneidensis* strain carrying a constitutive *sfgfp* plasmid driven by P_{trc*}. As expected, the three buffer gates each exhibited characteristic 'turn-on' response functions, where REU values increased in the presence of increasing inducer concentration (Fig. 3a–c).

Next, we assessed how these buffer gate architectures tailored *mtrC* expression and subsequent gel formation in engineered *S. oneidensis* strains at different induction levels. Controllable EET activity of each strain at different induction levels was first confirmed via iron reduction and ferrozine assay before their use for hydrogel cross-linking[35] (Supplementary Fig. 4). Afterward, strains harboring each of the regulator–promoter pairs were induced to varying extents following inoculation into a network precursor solution and the storage moduli of the resulting gels were measured. Gel stiffness increased concomitantly with inducer concentration across all Buffer gate circuits, except when the inducer–circuit combination yielded REU values above roughly 0.2–0.3. For the LacI and LuxR buffer gates, which operated below this REU bound, gel mechanics fit well to gene expression models and exhibited higher dynamic ranges, spanning a roughly 1,000-fold range in mechanical properties (Fig. 3a,b,f,g). However, the first iteration of the TetR buffer gate yielded transcriptional output above this range across all ATC concentrations, and subsequently no inducible control over gel properties was observed (Extended Data Fig. 3). Highlighting the design–test–build cycle for our parameterized circuits, we cloned several fluorescent constructs with varying ribosome binding site (RBS) strength for the TetR repressor[37]. These modified designs yielded REU values below roughly 0.2–0.3. When *sfgfp* was swapped for *mtrC*, increased inducer concentration was predictably correlated with stronger gels (Fig. 3c,h). Notably, the Hill function between storage modulus and inducer concentration closely mirrored each REU-parameterized gate. Normalized fluorescence and normalized material stiffness were also correlated across a range of inducer concentrations and gate architectures (Fig. 3j). The relative agreement between gel modulus and fluorescence and/or REU across the regulator–promoter pairs indicates similar transcriptional regulation when using *mtrC* or *sfgfp* as the output gene and validates future efforts toward forward engineering of material properties from established gene expression models. Together, these results demonstrate that well-characterized inducers and regulators can activate *mtrC*-driven gel formation and highlight useful design rules within our platform for establishing transcriptional control over network formation using MtrC.

https://doi.org/10.1038/s41589-024-01628-y

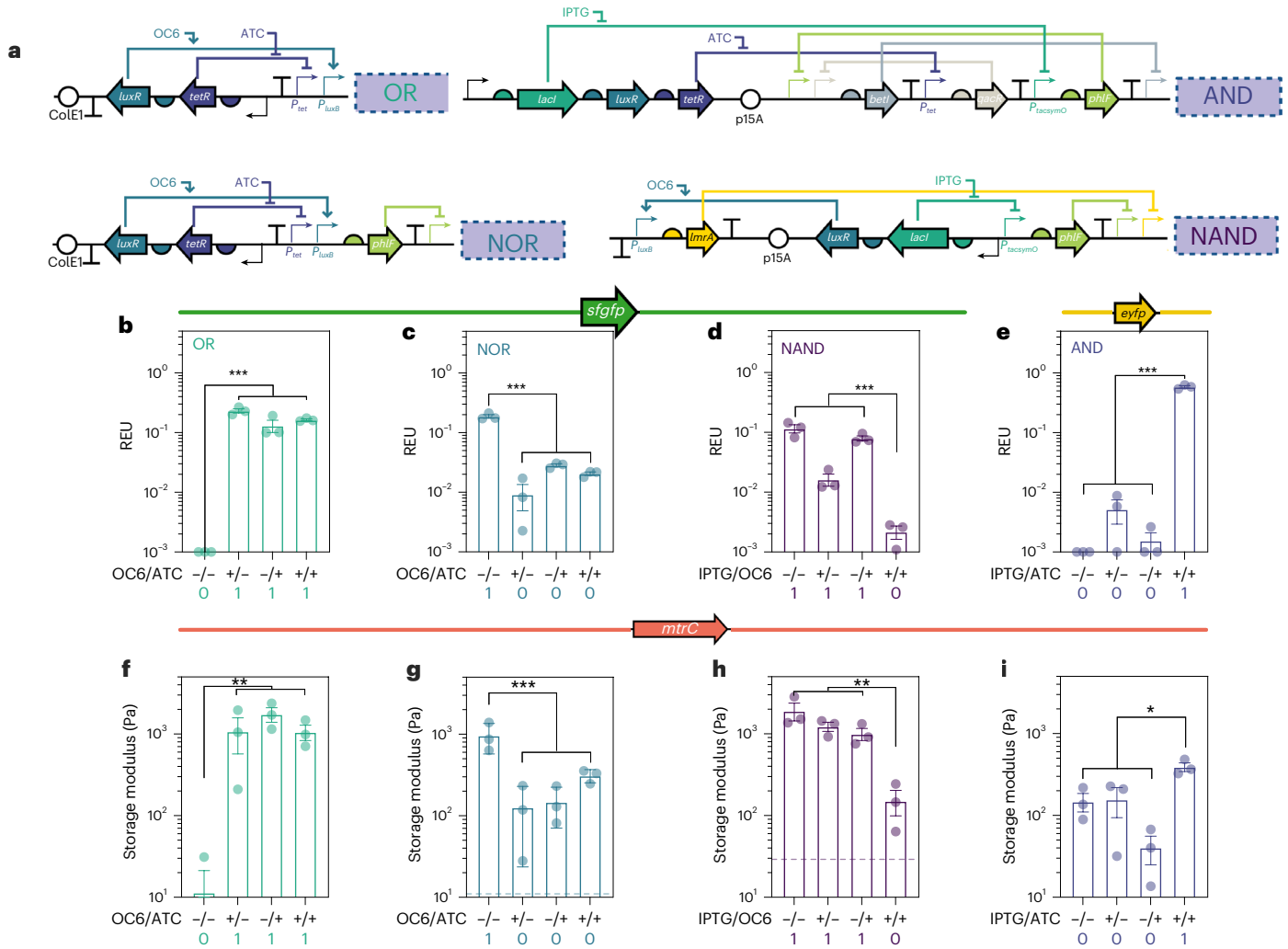

Fig. 4 | Genetic Boolean logic enables polymer network computation via living cellular actuators. a, Logical architectures with nested repressors coordinate expression of either *sfgfp* or *mtrC* using Boolean logic (OR, NOR, AND and NAND). The expected truth table are represented below each graph for the corresponding circuit (0, 'OFF'; 1, 'ON'). The repressors are activated or deactivated in response to their cognate inducing molecules (100 µM IPTG, 100 nM OC6 and 10 nM ATC). Created with Biorender.com. **b**–**e**, Relative gene expression (REU) of Boolean logic circuits controlling *sfgfp* or *eyfp*: OR (**b**), NOR (**c**), NAND (**d**) and AND (**e**). **f**–**i**, Storage modulus measured 24 h after inoculation with cells containing Boolean logic circuits controlling mtrC: OR (**f**), NOR (**g**), NAND (**h**) and AND (**i**). Dashed lines represent gel mechanics using corresponding knockout strains harboring an *sfgfp* vector as the control; if no line is shown, knockout strain gels did not form. Statistics performed are the results of a general linear hypothesis test (a contrast test) between the 'OFF' and 'ON' states. $^{*}P < 0.05$, $^{**}P < 0.01$, $^{***}P < 0.001$. R script is provided in the 'Data availability' section, and data shown are mean ± s.e.m. of $n = 3$ biological replicates.

To enable more complex logical operations, we next used transcriptional regulation to repress *mtrC* expression and switch off polymerization activity associated with EET flux. Turning off EET flux by negatively regulating MtrC, whose turnover rate exceeds the timescale of cell division (half-life roughly 16 h)[38,39], is challenging because previously expressed protein can only be removed via growth-driven dilution. An additional challenge to our system is that this residual MtrC can activate polymerization; thus, cell growth and protein dilution must also outcompete polymerization kinetics. To address these challenges, we predicted that a low inoculating optical density at 600 nm (OD_{600}) (~0.01) and longer reaction time (24 h) would enable coordinated transcriptional repression of the *mtrC* gene and attenuation of cross-linking activity. Specifically, we examined a dual-regulator NOT gate, which represses *mtrC* transcription and EET activity in response to IPTG, for hydrogel formation[35]. The NOT gate was constructed with *sfgfp* and *mtrC* as transcriptional outputs and response curves were measured for both strains. We found that networks cross-linked by *S. oneidensis* carrying this NOT gate formed weaker gels in response to increasing IPTG concentration, confirming dynamic repression of EET and resultant material mechanics (Fig. 3d,i). The response function of our NOT gate also confirmed that EET could be turned off only when REU values in the *sfgfp* circuit were tuned below 0.2–0.3. Despite the increase in regulation modules on the NOT gate circuit, the agreement between normalized fluorescence and storage modulus for the NOT gate was similar to that seen with the buffer gates (Fig. 3j). These results confirm that dynamic hydrogel formation can be transcriptionally turned off in response to an exogenous signal.

Boolean logic programs polymer network dynamics

The successful control of hydrogel mechanics using different buffer and NOT gate architectures suggested that *S. oneidensis* could be engineered to regulate polymer network synthesis through more complex logical operations. To demonstrate this, we created genetic two-input Boolean logic based on nested repressor architectures to control *mtrC*

expression and associated cross-linking[34,36,40,41] (Fig. 4). Each gate was designed with a sensing block using combinations of the one-input regulators described above and could be controlled via induction using common small molecule inducers. Specifically, we used OC6 and ATC sensors for OR and NOR gates, IPTG and ATC sensors for AND gates, and IPTG and OC6 sensors for NAND gates (Fig. 4). These sensor blocks control activation and deactivation of various repressor proteins, which coordinate to yield the desired gate-dependent transcriptional output. Before using the circuits to control *mtrC* expression and material properties, we first functionally validated each circuit in *S. oneidensis* using a fluorescent reporter. Starting with the simplest architecture, the OR gate was functionally validated using *sfgfp* fluorescence, where the 'ON' state occurred as expected in the presence of either or both inducers (OC6 and ATC) (Fig. 4b). Fluorescence in this gate could be controlled over several orders of magnitude. Increasing in genetic architecture complexity, the NOR gate turned 'OFF' in the presence of either or both inducers (Fig. 4c). The NAND gate, which is only 'ON' in the absence of both inducers, showed similar functional agreement (Fig. 4d). Each of these respective circuits performed with 'OFF' REU values below 0.2–0.3, suggesting their potential to tune polymer network mechanics based on our previous Buffer gate results. The most complex genetic regulation we tested, the AND gate, requires both inducers to be present to turn 'ON' (Fig. 4e). Using a previously developed AND architecture[40] that outputs *eyfp* (a yellow fluorescent reporter), we converted fluorescent values to REU by using a constitutive *eyfp* plasmid. Based on its function, we predicted the AND circuit should also be capable of toggling *mtrC* expression 'ON' and 'OFF'. Finally, each gate was responsive to changing inducer concentrations as indicated by gradients in REU represented in two-dimensional heat maps (Extended Data Fig. 4). Thus, we confirmed the expected truth tables for each genetic Boolean architecture and functionally validated many repressor proteins not previously tested in *S. oneidensis*.

We then placed *mtrC* under genetic Boolean regulation and applied these engineered strains toward polymer network cross-linking. Gates were tested under both stationary phase and dynamic cross-linking conditions. In all cases, resultant storage modulus followed the Boolean truth table for each logic operation (Fig. 4 and Extended Data Fig. 5). The OR gate, which was the simplest two-input architecture, exhibited the greatest dynamic range in storage modulus (roughly 100-fold). NOR, NAND and AND gates exhibited dynamic ranges of around three to tenfold, likely due to their increase in architectural complexity compared to the OR gate. The inducer-dependent outputs from the AND and NAND gates matched well with previous reports that used these specific architectures[40], including greater overall transcription in the NAND gate and decreased dynamic range in the AND gate. Strains harboring each circuit showed no measurable growth defect (Extended Data Fig. 6), supporting the role of EET-driven gel formation over unintended circuit effects that affect cellular physiology. Gated regulation of EET was also validated in separate Fe(III) reduction assays (Extended Data Fig. 7). Finally, cross-linking reactions in the presence of EET-deficient strains harboring induced fluorescent vectors produced significantly weaker gels, or no gels at all, compared to *mtrC*-expressing strains. Overall, logical computation in *S. oneidensis* using these two-input gates rationally tuned dynamic polymer network mechanics, highlighting transcriptional EET regulation as a viable method for programmable material computation in response to environmental signals.

EET actuates an orthogonal cross-linking chemistry

A notable advantage of using EET to control cross-linking is the genetically controllable interface between EET proteins and the metal catalyst, as opposed to the polymerized substrates. The ability to control many different redox chemistries using the same protein machinery could afford a greater degree of substrate modularity compared to living materials formed using proteins, nucleic acids, or enzymatically degradable linkers. Thus, we examined whether our EET-regulating circuits could be co-opted to control alternative metal-catalyzed reactions and cross-linking chemistries. Based on previous work involving small molecule synthesis, we predicted that *S. oneidensis* could transcriptionally regulate polymer cross-linking via CuAAC[42]. CuAAC is a ubiquitous biorthogonal cross-linking reaction that accesses unique polymer network structures compared to radical polymerizations[43,44]. Using four-arm alkyne- and azide-functionalized PEG macromers (Fig. 5a), we first demonstrated that CuAAC cross-linking could be driven by EET-capable *S. oneidensis* strains, and that resultant hydrogel mechanics were genetically encoded via *mtrC* expression (Supplementary Fig. 5). After establishing this link, we investigated single-input transcriptional control using buffer and NOT gate architectures controlling *mtrC* expression. The response function for each gate exhibited the predicted behavior and, just as in the case of ATRP, the regulation of EET activity in response to an inducer enabled control over CuAAC hydrogel mechanics (Fig. 5b,c). Together, these results establish that transcriptionally regulated electron flux from *S. oneidensis* can effectively regulate multiple cross-linking chemistries.

Given that *mtrC* expression could predictably control CuAAC activity, we predicted that this cross-linking mechanism could also mechanically regulate hydrogels using our genetic Boolean logic constructs without requiring amendment to the genetic architecture. Indeed, gels formed dynamically in response to appropriate environmental inputs and followed the expected transcriptional logic for each of the OR, NOR, AND and NAND gates (Fig. 5d–g). Network transformations generally exhibited greater dynamic range compared to radical polymerization, with accelerated cross-linking kinetics (12 h). The only exception was the AND gate, where transcriptional differences were possibly muted by rapid CuAAC kinetics[42,45] (Fig. 5g) and the complexity of the regulatory architecture. In all cases, gels did not form on this timescale in the presence of induced empty vector controls. Ultimately, successful circuit function to form CuAAC cross-linked gels demonstrates the modularity of EET for catalyzing diverse synthetic chemistries and living materials.

Logic-driven materials regulate fibroblast morphology

Mammalian cells are highly sensitive to the properties of the extracellular matrix, and hydrogel stiffness, viscoelasticity and other properties can drive cellular behaviors including spreading, differentiation and migration[46–48]. One potential application for ELMs is the ability to program mechanical or compositional changes in tissue engineering scaffolds that lead to phenotypic or morphological changes for cells. For example, human mesenchymal stem cell adhesion could be induced by ELMs created from the overexpression of a fibronectin protein in *Lactococcus lactis*[49]. These studies highlight the potential use of bacteria as actuators of biomaterials in multi-domain consortia. To exemplify how EET could serve as a computational conduit for such scaffolds, we explored whether transcriptional logic programmed into *S. oneidensis* could ultimately dictate mammalian cell behavior via control over material properties. Thus, we hypothesized that Boolean logic driving EET would create gels of different stiffnesses, and that this would in turn drive differences in actin polymerization within fibroblasts seeded on these gels (Fig. 6a). To this end, we used engineered *S. oneidensis* harboring each gate to cross-link PEG-methacrylate hydrogels supplemented with commercial gelatin-methacrylate for adherence. Gels were allowed to swell overnight before seeding human-derived dermal fibroblasts on the gel surface. F-actin was stained using rhodamine phalloidin and nuclei were stained with DAPI (4,6-diamidino-2-phenylindole), enabling measurements of single cells to be collected (Fig. 6b–e). We observed that fibroblasts were less circular on hydrogels that were predicted to be stiffer, or 'ON', based on the corresponding Boolean logic encoded in the engineered *S. oneidensis* strain. By contrast, hydrogels that were predicted to be softer, or 'OFF', yielded fibroblasts that were more circular. Cell spreading was

https://doi.org/10.1038/s41589-024-01628-y

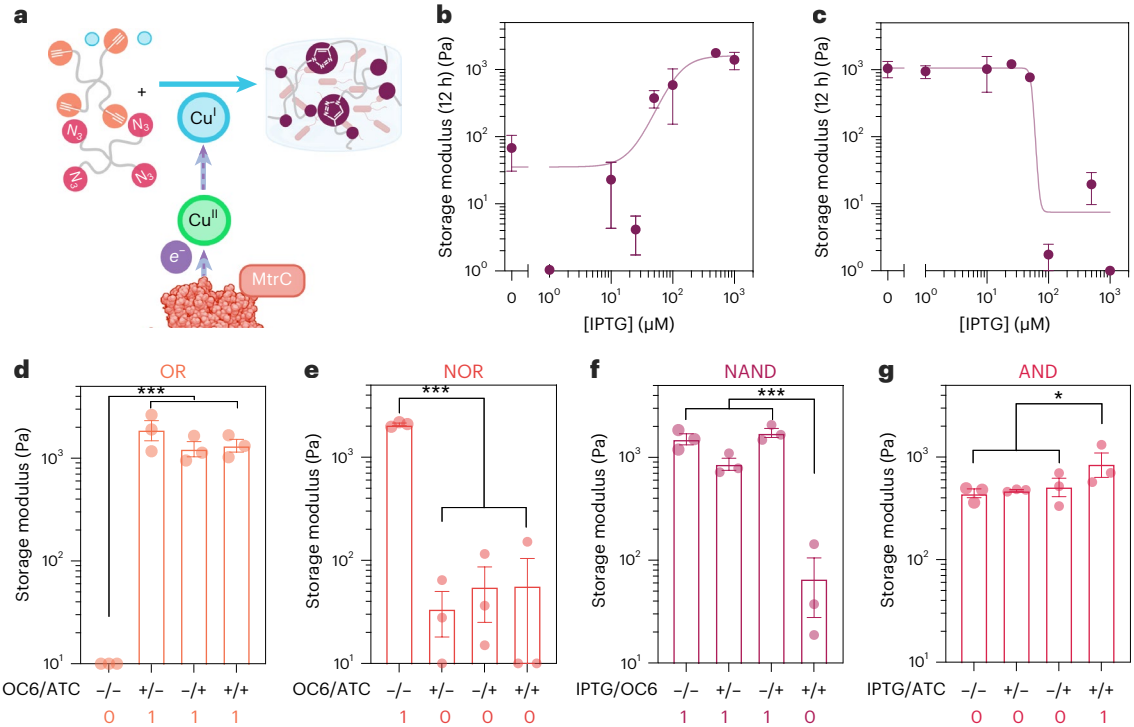

Fig. 5 | Alternative living material chemistries enabled by EET-driven CuAAC cross-linking. a, Schematic indicating cross-linking between four-arm alkyne and azide polymers to yield mechanically regulated triazole polymer network. Created with Biorender.com **b**,**c**, CuAAC cross-linked polymer networks can be transcriptionally regulated via EET using buffer (**b**) and NOT gate (**c**) architectures. Data shown are mean ± s.e.m. of $n = 3$ biological replicates. **d**–**g**, Genetic Boolean logic enables cross-linking via *mtrC* expression for OR (**d**), NOR (**e**), NAND (**f**) and AND (**g**) architectures. In all cases storage modulus was measured 12 h after inoculation. The expected truth tables are represented below each circuit (0, 'OFF'; 1, 'ON'). Statistics performed are the results of a general linear hypothesis test (a contrast test) between the 'OFF' and 'ON' states. $^*P < 0.05$, $^{**}P < 0.01$, $^{***}P < 0.001$. R script is provided in the 'Data availability' section, and data shown are mean ± s.e.m. of $n = 3$ biological replicates. A complete statistical summary is available in the Supplementary Information.

quantified as circularity, and plots of 1 − circularity also statistically followed the expected truth tables for each ON/OFF condition (Fig. 6f–i). Measurements for cell size reveal statistically significant differences between the logic conditions except for NAND (Supplementary Fig. 6). Together, these data indicate that *S. oneidensis* can act as a cellular interface to translate transcriptional logic to morphologic changes in fibroblasts via ELMs.

Discussion

By linking metabolic function to synthetic cross-linking catalysts, we created a generalizable platform for engineered living material synthesis that capitalizes on the diverse computational power of transcriptional logic. Specifically, we developed dynamic cross-linking reactions where living cells respond to dilute environmental signals and initiate macroscopic polymer network formation, emulating natural processes such as biofilm and tissue formation. Our on-demand system leveraged a small initial inoculum of cells ($OD_{600} \approx 0.01$–0.05) and could actuate large material changes (roughly 1–1,000 Pa) without previous expression of EET proteins. Materials cross-linked using stationary phase conditions performed similarly; however, dynamic systems coupling microbial sensing, computation, and actuation in a single reaction more closely approximate natural materials. In addition, dynamic cross-linking suppressed background reactivity and enabled naïve bacteria to initiate reactions at later times via oxygen inhibition. Placing several EET-relevant genes under simple transcriptional buffer gates (within their cognate genomic knockout strains) demonstrated that multiple biological handles control cross-linking rate and final modulus. Ultimately, we found that the terminal EET protein in the Mtr-pathway, MtrC, provided the most convenient engineering target and that MtrC expression was directly correlated with material mechanics. In addition to transcriptional control, gel stiffness could be further tuned by altering reaction time and inoculation density. Our system responds in real-time to dilute chemical signals and ultimately links transcriptional changes to macroscopic synthetic material properties.

Synthetic biologists have established numerous paradigms for programming living systems, including computation using genetic logic; however, most have focused on fluorescence as an output. In contrast to standard fluorescent reporters, MtrC is directly involved in anaerobic cell metabolism, a member of a multi-protein membrane-bound protein pathway (MtrCAB) and notably larger (78.45 versus 26.8 kDa for sfGFP). Thus, circuits that regulate MtrC and EET are challenging to predictably design[50]. To enable a smoother feed-forward design process, we developed a metrology for predicting the effect of controlling MtrC levels on material formation by comparing to fluorescent reporter circuits. Specifically, we characterized several buffer gates in *S. oneidensis* using both *sfgfp* and *mtrC* expression as outputs and concentration-dependent gradients in both gene expression (REU) and living material mechanics (storage modulus, G'). While REU uses fluorescence to indirectly measure matured protein concentration, our gel storage modulus measurement is a result of multiple simultaneous processes including protein expression, cell growth, oxygen consumption, catalyst reduction and polymerization kinetics. Despite the various timescales and mechanisms of these processes, both REU and the storage modulus outputs could be represented as activating Hill functions, indicating robust transcriptional control over hydrogel formation and mechanics. Indeed, we found that gel stiffness could be predictably varied over several orders of magnitude using relatively simple transcriptional circuits. Our observation that storage moduli fit well to characteristic gene expression models is supported by established theory in that during exponential growth,

https://doi.org/10.1038/s41589-024-01628-y

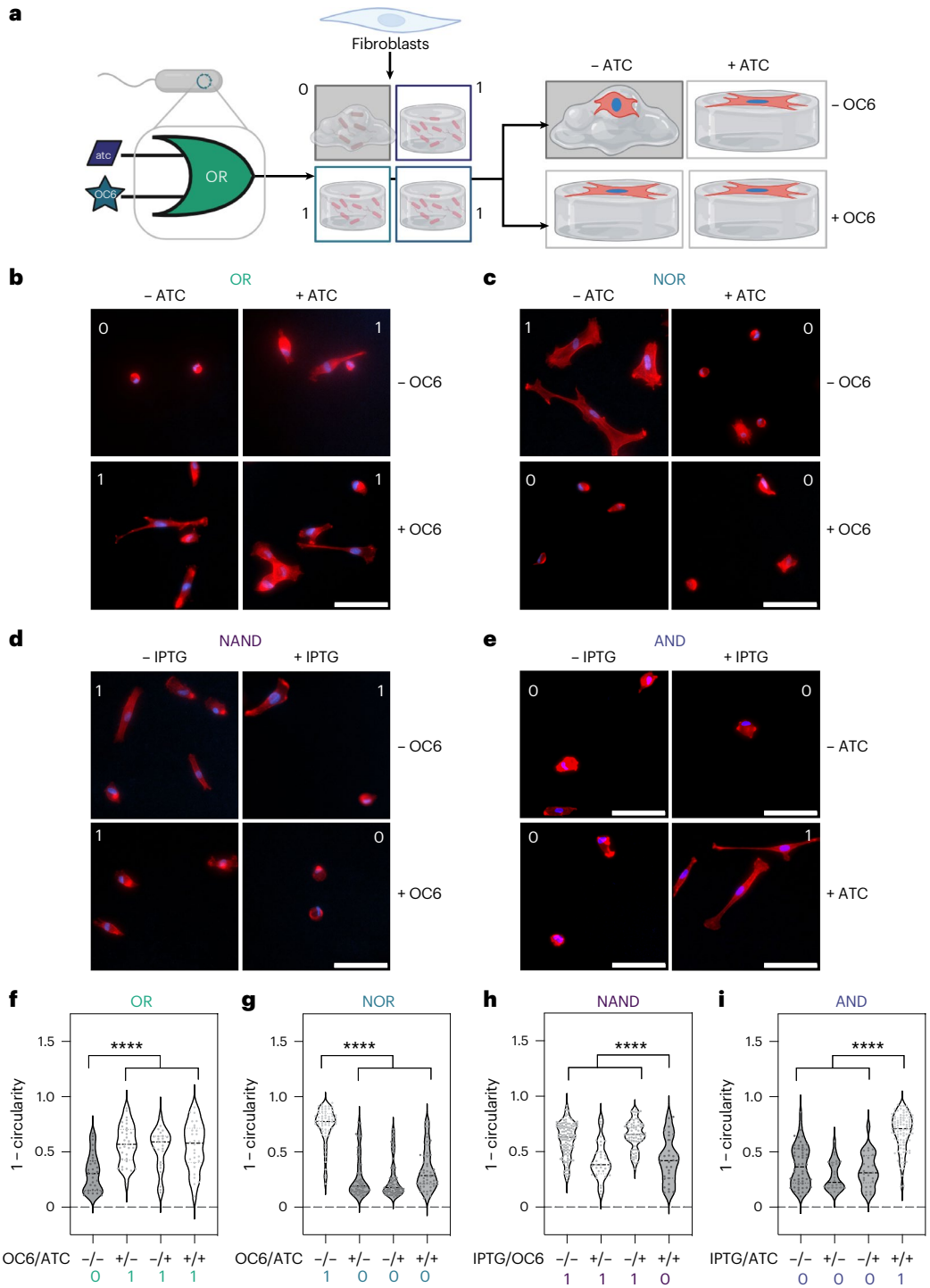

Fig. 6 | Fibroblast morphology is dictated by living material mechanics under genetic Boolean regulation. a, Schematic demonstrating workflow for creating EET-regulated hydrogels and seeding of dermal fibroblasts. Boolean logic programs cross-linking via *mtrC* expression, yielding changes in living material stiffness, which subsequently drives fibroblast spreading and circularity (measured as $4\pi(\text{area/perimeter}^2)$). Created with Biorender.com. **b**–**e**, Epifluorescence microscopy images of fibroblasts seeded on hydrogels for 18–20 h stained with rhodamine phalloidin (red) and with DAPI (blue) for each cross-linking condition for OR (**b**), NOR (**c**), AND (**d**) and NAND (**e**) gates. Scale bars, 100 µm. **f**–**i**, Fibroblast circularity as a function of Boolean logic driving hydrogel cross-linking via EET for OR (**f**), NOR (**g**), NAND (**h**) and AND (**i**) architectures. Measurements came from only particles containing a single-nuclei and were collected from either two or three hydrogels for each condition, no fewer than 25 particles per condition. The expected truth tables are represented below each circuit (0, 'OFF'; 1, 'ON') and the *y* axis was chosen as 1 − circularity such that '0' represents both 'OFF' and correlates to a perfect circle. Statistics performed are the results of a general linear hypothesis test (a contrast test) between the 'OFF' and 'ON' states. $^{*}P < 0.05$, $^{**}P < 0.01$, $^{***}P < 0.001$, $^{****}P < 0.0001$. R script is provided in the 'Data availability' section, and a complete statistical summary is available in the Supplementary Information.

protein concentrations should approach steady state[51,52], presumably leading to consistent EET rates. We note that our parametrization of EET gene expression used REU fluorescence measurements taken at stationary phase and that these values likely differ during early exponential growth in gels. Nonetheless, our REU metrology yielded useful performance metrics for hydrogel formation as a function of inducer concentration and established an approximately linear correlation between fluorescence and storage modulus. Most notably, we discovered that REU values in our system should be kept below around 0.2–0.3 for a tunable polymer network response. This was best demonstrated in the development of TetR–P_{Tet} response curves, where the original circuit strength yielded minimal differences in functional output, and REU parameterization facilitated the design–test–build cycle via ribosome binding site engineering. Overall, our results suggest that traditional REU measurements of fluorescent reporter circuits can be leveraged to draw parallels to the general behavior of storage modulus in living materials created using transcriptional regulation of EET genes.

Leveraging the genetic circuit metrology developed for our buffer gate experiments, we attenuated cross-linking in response to increasing inducer concentration by repressing MtrC expression in our NOT gate[35]. This result is particularly notable as the repression of *mtrC* and the dilution of any previously expressed protein must outcompete both EET-driven and background cross-linking reactions. Despite these challenges, the NOT gate exhibited the predicted response in EET-driven cross-linking. We speculate that the NOT gate functions as designed for two critical reasons. First, we previously showed that cross-linking and polymerization activity is proportional to the size of the initial cell population and the small initial cell inoculum limits the extent of cross-linking at early time points. Second, cells must first consume dissolved oxygen in solution, as it can quench radicals and deactivate the copper catalyst. We previously demonstrated that EET-driven reactions require the cell population to reach a critical density to outcompete oxygen mass transfer[30,31,42]. Consequently, at low cell densities, oxygen likely quenches cross-linking until the cell population grows to a critical density, after which *mtrC* has been repressed via the NOT gate and previously expressed protein has been sufficiently diluted to observe the desired logic response. The successful implementation of the NOT gate for regulating cross-linking enabled more sophisticated logic operations to be applied to EET-driven material synthesis.

Indeed, we found that four common Boolean operators OR, NOR, AND and NAND could be designed using off-the-shelf genetic parts to rationally control EET activity and resultant cross-linking. To our knowledge, these results represent the most comprehensive demonstration of two-input logic gates regulating EET flux and are a striking example of how transcriptional regulation of EET proteins can enable genetic control of extracellular redox chemistries[53]. Such chemistries are typically considered inaccessible by biology and represent an emerging class of living synthetic reactions and materials. Material cross-linking using bacterial strains containing the two-input circuits performed as expected based on the two-input fluorescent truth tables. We did observe heterogeneity in gate performance and dynamic range depending on circuit identity. The simplest gates, containing one or two repressors, exhibited the greatest dynamic range in storage modulus. Gates with more repressors (AND and NAND) showed decreased dynamic range. These results are consistent with the limitations of nested repressor architectures, as each additional repressor requires protein build-up in the cell to activate the next part of the circuit. Our results are also consistent with the observation that nested transcriptional architectures are generally not favored by natural systems to control time-dependent processes requiring fast dynamics[54]. In addition to the complexity of the circuit, other factors including leaky gene expression, metabolic burden and nonspecific catalyst activation can affect gate performance in our system. For example, cross-linking can occur independently of transcriptional regulation via background radical production or adventitious catalyst reduction (for example via flavins, MtrA). By contrast, fluorescent reporters exhibit fewer competing background fluorescent processes that can contribute to system noise. We hypothesize that these processes explain the differences in dynamic range and overall response when comparing hydrogel mechanics to fluorescence measurements. Fortunately, we found that even relatively complex transcriptional regulation could still outcompete background reduction–polymerization and leaky expression to yield the predicted output. Future improvements in the dynamic range of hydrogel modulus could be realized by applying recent advancements in genetic circuit standardization and assembly, such as gate matching[40] or antirepressors[55]. Overall, our platform provides a foundation for bridging multi-scale temporal and spatial processes using synthetic and systems biology-inspired material design.

As a demonstration of our system's modularity, we applied EET-based logic to an orthogonal chemistry, CuAAC. This chemical reaction uses a different catalyst and monomers compared to our previous radical polymerization platforms, but could still be genetically and transcriptionally regulated due to the control over metal redox state. Specifically, increased *mtrC* expression was correlated with stronger gels and CuAAC gel mechanics were consistent with the expected truth tables when formed with strains harboring Boolean regulators of *mtrC*. CuAAC gels exhibited high dynamic range with the simpler gates (OR and NOR), yielding responses that matched their fluorescent counterparts. The NAND gate also exhibited high dynamic range between ON and OFF conditions for CuAAC cross-linked gels. We observed a lower dynamic range for the higher complexity AND gate, but the resulting difference in mechanics between ON and OFF states was still statistically significant. The differences in gate performance between radical polymerization- versus CuAAC-formed gels are likely due to the different mechanisms of cross-linking (step- versus chain-growth) necessary to form gels using the respective chemistries. In contrast to ATRP, CuAAC does not have a reversible catalyst deactivation step, likely contributing to more rapid kinetics than ATRP cross-linked gels. This appeared to improve dynamic range in simpler systems with fewer repressors, but also may have contributed to higher background signal and lower dynamic range for more complex circuits. Nevertheless, the ability to exert biological control over different chemistries using identical genetic machinery suggests that EET can serve as a modular actuator for other synthetic redox reactions, providing a platform for combining biomaterial engineering, organometallic chemistry and synthetic biology[9]. Thus, our use of EET actuation vastly broadens the substrate scope available to biological systems and allows fully synthetic redox reactions to control living material properties.

Relative to purely chemical systems, our platform responds to very low input magnitudes (nanomolar to micromolar) and amplifies this signal to affect a macroscopic material transformation spanning a roughly 1,000-fold mechanical range. The living materials field is increasingly capitalizing on diverse biological sensing and computation to manipulate traditionally inert systems. Our system demonstrates how noncongruent logic (OR versus NOR or AND versus NAND) can be actuated on the same material via this transcriptional interface, without requiring further material synthesis. Furthermore, the use of two orthogonal chemistries (CuAAC and ATRP) demonstrates that this engineering strategy is not limited to a single chemical system but instead maintains a high degree of modularity. While responsive materials that use DNA[22] or curli fibers[10,11] modulate preformed synthetic hydrogels[14,16] or rely on endogenous host-synthesized materials[56] or cell lysis[57], our system allows for robust metabolic and/or genetic control over potentially any biologically compatible material capable of radical or CuAAC cross-linking. For example, our general strategy can be applied to simple off-the-shelf monomers, common tissue engineering scaffolds[19], or cells functionalized with noncanonical amino acids[22,58].

We leveraged this capability to apply transcriptionally regulated living material mechanics to drive fibroblast morphology[46,47,59]. Stiffer hydrogels, programmed by Boolean computation to correspond to the 'ON' EET state, yielded distinct fibroblast morphology relative to the 'OFF' state. We saw that in all cases, our transcriptional logic directly predicted cell circularity using only EET activity. Further work investigating the interactions between the embedded bacteria and the immune response, cytokine release and cell viability is required[60–63]; however, the ability to program cell morphology via bacterial genetic logic and material properties may find applications in wound or tissue repair[64,65], biosensing[22], drug delivery[25] and for modeling interfaces between prokaryotes and eukaryotes.

We also note that our microbially driven cross-linking reactions are orthogonally compatible with a wide range of other biologically generated materials including biomineralized carbonates[66], cellulose[67] and curli fibers[12]. Relative to other examples of ELMs, connecting EET flux to an organometallic output vastly broadens the scope of inputs and computations that can regulate a cross-linking event, including specific DNA–RNA sequences[54,55], clinical biomarkers[68], environmental contaminants[69] or combinations of these stimuli. Finally, the genotype–phenotype link between EET protein expression and hydrogel properties implies that cross-linkable materials are controllable using alternative forms of genetic regulation, including CRISPR[68], riboswitches[69] or integrases[70]. Overall, our results demonstrate the modularity EET-based systems offer for controlling a range of material chemistries, while maintaining their compatibility with existing genetic circuit diversity and other ELM technologies.

By leveraging electron transfer from living actuators that affect synthetic polymer network chemistry, we addressed many limitations of living materials and integrated the full suite of synthetic biology tools (for example, sensors, regulators and computational machinery) for bottom-up materials design. Specifically, we developed a workflow for generating genetically programmable and stimuli-responsive living synthetic materials through the biological interface of EET. Our design's modularity in both genetic circuitry and network chemistry holds promise for intervention-less and responsive cross-linking platforms, where engineered microbes can be incorporated into tissue architectures, biosensors, soft actuators or additive manufacturing substrates. As even relatively small changes in local micromechanics are crucial in living systems, transcriptionally tuning within this window may open biomimetic opportunities for functional living materials. Overall, our work provides the foundation for applying the genetic regulatory motifs found in patterning, embryogenesis and tissue formation toward the control of synthetic polymer networks.

Online content

Any methods, additional references, Nature Portfolio reporting summaries, source data, extended data, supplementary information, acknowledgements, peer review information; details of author contributions and competing interests; and statements of data and code availability are available at https://doi.org/10.1038/s41589-024-01628-y.

References

1. Martyn, I. & Gartner, Z. J. Expanding the boundaries of synthetic development. *Dev. Biol.* **474**, 62–70 (2021).
2. Luo, N., Wang, S. & You, L. Synthetic pattern formation. *Biochemistry* **58**, 1478–1483 (2019).
3. Sirisaengtaksin, N., Odem, M. A., Bosserman, R. E., Flores, E. M. & Krachler, A. M. The *E. coli* transcription factor GrlA is regulated by subcellular compartmentalization and activated in response to mechanical stimuli. *Proc. Natl Acad. Sci. USA* **117**, 9519–9528 (2020).
4. Goodwin, K. & Nelson, C. M. Mechanics of development. *Dev. Cell* **56**, 240–250 (2021).
5. Humphries, J. et al. Species-independent attraction to biofilms through electrical signaling. *Cell* **168**, 200–209.e12 (2017).
6. Roth, J. G. et al. Advancing models of neural development with biomaterials. *Nat. Rev. Neurosci.* **22**, 593–615 (2021).
7. Kholodenko, B. N. Cell-signalling dynamics in time and space. *Nat. Rev. Mol. Cell Biol.* **7**, 165–176 (2006).
8. Fern, J. & Schulman, R. Modular DNA strand-displacement controllers for directing material expansion. *Nat. Commun.* **9**, 3766 (2018).
9. Rodrigo-Navarro, A., Sankaran, S., Dalby, M. J., del Campo, A. & Salmeron-Sanchez, M. Engineered living biomaterials. *Nat. Rev. Mater.* **6**, 1175–1190 (2021).
10. Cao, Y. et al. Programmable assembly of pressure sensors using pattern-forming bacteria. *Nat. Biotechnol.* **35**, 1087–1093 (2017).
11. Praveschotinunt, P. et al. Engineered *E. coli* Nissle 1917 for the delivery of matrix-tethered therapeutic domains to the gut. *Nat. Commun.* **10**, 5580 (2019).
12. Duraj-Thatte, A. M. et al. Water-processable, biodegradable and coatable aquaplastic from engineered biofilms. *Nat. Chem. Biol.* **17**, 732–738 (2021).
13. Kang, S.-Y. et al. Engineering *Bacillus subtilis* for the formation of a durable living biocomposite material. *Nat. Commun.* **12**, 7133 (2021).
14. Smith, R. S. H. et al. Hybrid living materials: digital design and fabrication of 3D multimaterial structures with programmable biohybrid surfaces. *Adv. Funct. Mater.* **30**, 1907401 (2020).
15. Gilbert, C. et al. Living materials with programmable functionalities grown from engineered microbial co-cultures. *Nat. Mater.* **20**, 691–700 (2021).
16. Rivera-Tarazona, L. K., Campbell, Z. T. & Ware, T. H. Stimuli-responsive engineered living materials. *Soft Matter* **17**, 785–809 (2021).
17. González, L. M., Mukhitov, N. & Voigt, C. A. Resilient living materials built by printing bacterial spores. *Nat. Chem. Biol.* **16**, 126–133 (2020).
18. Graham, A. J. & Keitz, B. K. in *Engineered Living Materials* (ed. Srubar III, W. V.) 27–49 (Springer International, 2023).
19. Rosales, A. M. & Anseth, K. S. The design of reversible hydrogels to capture extracellular matrix dynamics. *Nat. Rev. Mater.* **1**, 15012 (2016).
20. Kaspar, C., Ravoo, B. J., van der Wiel, W. G., Wegner, S. V. & Pernice, W. H. P. The rise of intelligent matter. *Nature* **594**, 345–355 (2021).
21. Zhang, X. et al. The pathway to intelligence: using stimuli-responsive materials as building blocks for constructing smart and functional systems. *Adv. Mater.* **31**, 1804540 (2019).
22. English, M. A. et al. Programmable CRISPR-responsive smart materials. *Science* **365**, 780–785 (2019).
23. Zhang, H., Zeng, H., Priimagi, A. & Ikkala, O. Viewpoint: Pavlovian materials—functional biomimetics inspired by classical conditioning. *Adv. Mater.* **32**, 1906619 (2020).
24. Ikeda, M. et al. Installing logic-gate responses to a variety of biological substances in supramolecular hydrogel–enzyme hybrids. *Nat. Chem.* **6**, 511–518 (2014).
25. Badeau, B. A., Comerford, M. P., Arakawa, C. K., Shadish, J. A. & DeForest, C. A. Engineered modular biomaterial logic gates for environmentally triggered therapeutic delivery. *Nat. Chem.* **10**, 251–258 (2018).
26. Korevaar, P. A., Kaplan, C. N., Grinthal, A., Rust, R. M. & Aizenberg, J. Non-equilibrium signal integration in hydrogels. *Nat. Commun.* **11**, 386 (2020).
27. Daly, A. C., Prendergast, M. E., Hughes, A. J. & Burdick, J. A. Bioprinting for the biologist. *Cell* **184**, 18–32 (2021).
28. Rivera-Tarazona, L. K., Bhat, V. D., Kim, H., Campbell, Z. T. & Ware, T. H. Shape-morphing living composites. *Sci. Adv.* **6**, eaax8582 (2020).

29. Shi, L. et al. Extracellular electron transfer mechanisms between microorganisms and minerals. *Nat. Rev. Microbiol.* **14**, 651–662 (2016).
30. Fan, G., Graham, A. J., Kolli, J., Lynd, N. A. & Keitz, B. K. Aerobic radical polymerization mediated by microbial metabolism. *Nat. Chem.* **12**, 638–646 (2020).
31. Graham, A. J. et al. Genetic control of radical cross-linking in a semisynthetic hydrogel. *ACS Biomater. Sci. Eng.* **6**, 1375–1386 (2020).
32. Beliaev, A. S. et al. Gene and protein expression profiles of *Shewanella oneidensis* during anaerobic growth with different electron acceptors. *OMICS J. Integr. Biol.* **6**, 39–60 (2002).
33. Coursolle, D. & Gralnick, J. A. Reconstruction of extracellular respiratory pathways for iron(III) reduction in *Shewanella oneidensis* strain MR-1. *Front. Microbiol.* **3**, 56 (2012).
34. Brophy, J. A. N. & Voigt, C. A. Principles of genetic circuit design. *Nat. Methods* **11**, 508–520 (2014).
35. Dundas, C. M., Walker, D. J. F. & Keitz, B. K. Tuning extracellular electron transfer by *Shewanella oneidensis* using transcriptional logic gates. *ACS Synth. Biol.* **9**, 2301–2315 (2020).
36. Nielsen, A. A. K. et al. Genetic circuit design automation. *Science* **352**, aac7341 (2016).
37. Reis, A. C. & Salis, H. M. An automated model test system for systematic development and improvement of gene expression models. *ACS Synth. Biol.* **9**, 3145–3156 (2020).
38. Rosenfeld, N. & Alon, U. Response delays and the structure of transcription networks. *J. Mol. Biol.* **329**, 645–654 (2003).
39. Xiong, Y. et al. Targeted protein degradation of outer membrane decaheme cytochrome MtrC metal reductase in *Shewanella oneidensis* MR-1 measured using biarsenical probe CrAsH-EDT2. *Biochemistry* **50**, 9738–9751 (2011).
40. Stanton, B. C. et al. Genomic mining of prokaryotic repressors for orthogonal logic gates. *Nat. Chem. Biol.* **10**, 99–105 (2014).
41. Tamsir, A., Tabor, J. J. & Voigt, C. A. Robust multicellular computing using genetically encoded NOR gates and chemical 'wires'. *Nature* **469**, 212–215 (2011).
42. Partipilo, G., Graham, A. J., Belardi, B. & Keitz, B. K. Extracellular electron transfer enables cellular control of Cu(I)-catalyzed alkyne–azide cycloaddition. *ACS Cent. Sci.* https://doi.org/10.1021/acscentsci.1c01208 (2022).
43. Gao, H., Chan, N., Oh, J. K. & Matyjaszewski, K. in *In-Situ Gelling Polymers* (ed. Loh, X. J.) 69–105 (Springer, 2014).
44. Tibbitt, M. W., Kloxin, A. M., Sawicki, L. & Anseth, K. S. Mechanical properties and degradation of chain and step polymerized photodegradable hydrogels. *Macromolecules* **46**, 2785–2792 (2013).
45. Adzima, B. J. et al. spatial and temporal control of the alkyne–azide cycloaddition by photoinitiated Cu(II) reduction. *Nat. Chem.* **3**, 256–259 (2011).
46. Hillsley, A., Santos, J. E. & Rosales, A. M. A deep learning approach to identify and segment alpha-smooth muscle actin stress fiber positive cells. *Sci. Rep.* **11**, 21855 (2021).
47. Tomasek, J. J., Gabbiani, G., Hinz, B., Chaponnier, C. & Brown, R. A. Myofibroblasts and mechano-regulation of connective tissue remodelling. *Nat. Rev. Mol. Cell Biol.* **3**, 349–363 (2002).
48. Chaudhuri, O., Cooper-White, J., Janmey, P. A., Mooney, D. J. & Shenoy, V. B. Effects of extracellular matrix viscoelasticity on cellular behaviour. *Nature* **584**, 535–546 (2020).
49. Hay, J. J. et al. Bacteria-based materials for stem cell engineering. *Adv. Mater.* **30**, 1804310 (2018).
50. Su, L., Fukushima, T. & Ajo-Franklin, C. M. A hybrid cyt C maturation system enhances the bioelectrical performance of engineered *Escherichia coli* by improving the rate-limiting step. *Biosens. Bioelectron.* **165**, 112312 (2020).
51. Klumpp, S., Zhang, Z. & Hwa, T. Growth rate-dependent global effects on gene expression in bacteria. *Cell* **139**, 1366–1375 (2009).
52. Zhang, H. M. et al. Measurements of gene expression at steady state improve the predictability of part assembly. *ACS Synth. Biol.* **5**, 269–273 (2015).
53. Hu, Y., Yang, Y., Katz, E. & Song, H. Programming the quorum sensing-based AND gate in shewanella oneidensis for logic gated-microbial fuel cells. *Chem. Commun. Camb. Engl.* **51**, 4184–4187 (2015).
54. Alon, U. *An Introduction to Systems Biology: Design Principles of Biological Circuits* 2nd edn (Chapman and Hall, 2019).
55. Groseclose, T. M., Rondon, R. E., Herde, Z. D., Aldrete, C. A. & Wilson, C. J. Engineered systems of inducible anti-repressors for the next generation of biological programming. *Nat. Commun.* **11**, 4440 (2020).
56. Molinari, S. et al. A de novo matrix for macroscopic living materials from bacteria. *Nat. Commun.* **13**, 5544 (2022).
57. Dai, Z. et al. Living fabrication of functional semi-interpenetrating polymeric materials. *Nat. Commun.* **12**, 3422 (2021).
58. Wang, F. et al. A biocompatible heterogeneous MOF–Cu catalyst for in vivo drug synthesis in targeted subcellular organelles. *Angew. Chem. Int. Ed.* **58**, 6987–6992 (2019).
59. Hinz, B., Mastrangelo, D., Iselin, C. E., Chaponnier, C. & Gabbiani, G. Mechanical tension controls granulation tissue contractile activity and myofibroblast differentiation. *Am. J. Pathol.* **159**, 1009–1020 (2001).
60. Witte, K., Rodrigo-Navarro, A. & Salmeron-Sanchez, M. Bacteria-laden microgels as autonomous three-dimensional environments for stem cell engineering. *Mater. Today Bio.* **2**, 100011 (2019).
61. Petaroudi, M., Rodrigo-Navarro, A., Dobre, O., Dalby, M. J. & Salmeron-Sanchez, M. Living biomaterials to engineer hematopoietic stem cell niches. *Adv. Healthc. Mater.* **11**, 2200964 (2022).
62. Lee, K. Y. & Mooney, D. J. Hydrogels for tissue engineering. *Chem. Rev.* **101**, 1869–1880 (2001).
63. Jeon, J. W., Cho, I. H., Ha, U. H., Seo, S. K. & Paek, S. H. Chemiluminometric immuno-analysis of innate immune response against repetitive bacterial stimulations for the same mammalian cells. *Sci. Rep.* **4**, 6011 (2014).
64. Schultz, G. S., Davidson, J. M., Kirsner, R. S., Bornstein, P. & Herman, I. M. Dynamic reciprocity in the wound microenvironment. *Wound Repair Regen.* **19**, 134–148 (2011).
65. Freedman, B. R. et al. Enhanced tendon healing by a tough hydrogel with an adhesive side and high drug-loading capacity. *Nat. Biomed. Eng.* https://doi.org/10.1038/s41551-021-00810-0 (2022).
66. Heveran, C. M. et al. Biomineralization and successive regeneration of engineered living building materials. *Matter* **2**, 481–494 (2020).
67. Caro-Astorga, J., Walker, K. T., Herrera, N., Lee, K.-Y. & Ellis, T. Bacterial cellulose spheroids as building blocks for 3D and patterned living materials and for regeneration. *Nat. Commun.* **12**, 5027 (2021).
68. Cubillos-Ruiz, A. et al. An engineered live biotherapeutic for the prevention of antibiotic-induced dysbiosis. *Nat. Biomed. Eng.* **6**, 910–921 (2022).
69. Karbelkar, A. A., Reynolds, E. E., Ahlmark, R. & Furst, A. L. A microbial electrochemical technology to detect and degrade organophosphate pesticides. *ACS Cent. Sci.* **7**, 1718–1727 (2021).
70. Green, A. A. et al. Complex cellular logic computation using ribocomputing devices. *Nature* **548**, 117–121 (2017).

Publisher's note Springer Nature remains neutral with regard to jurisdictional claims in published maps and institutional affiliations.

Springer Nature or its licensor (e.g. a society or other partner) holds exclusive rights to this article under a publishing agreement with the author(s) or other rightsholder(s); author self-archiving of the accepted manuscript version of this article is solely governed by the terms of such publishing agreement and applicable law.

© The Author(s), under exclusive licence to Springer Nature America, Inc. 2024

Methods

Chemicals and reagents

Here, four-arm 5k PEG-MA (≥95% functionalization, Advanced BioChemicals), copper(II) bromide ($CuBr_2$) (Sigma-Aldrich, 99%), TPMA (Sigma-Aldrich, 98%), tris(benzyltriazolylmethyl)amine (THPTA) (Sigma-Aldrich, 95%), 2-(4-((bis((1-(*tert*-butyl)-1*H*-1,2,3-triazol-4-yl) methyl)amino)methyl)-1*H*-1,2,3-triazol-1-yl)acetic acid (BTTAA) (Click Chemistry Tools >95%), HEBIB (Sigma-Aldrich, 95%), sodium DL-lactate ($NaC_3H_5O_3$) (TCI, 60% in water), sodium fumarate ($Na_2C_4H_2O_4$) (VWR, 98%), HEPES buffer solution ($C_8H_{18}N_2O_4S$) (VWR, 1 M in water, pH 7.3), potassium phosphate dibasic (K_2HPO_4) (Sigma-Aldrich), potassium phosphate monobasic (KH_2PO_4) (Sigma-Aldrich), sodium chloride (NaCl) (VWR), ammonium sulfate ($(NH_4)_2SO4$) (Fisher Scientific), magnesium(II) sulfate heptahydrate ($MgSO_4{\cdot}7H_2O$) (VWR), trace mineral supplement (American Type Culture Collection), casamino acids (VWR), IPTG (Teknova), ATC (Sigma-Aldrich), OC6 (Sigma-Aldrich), kanamycin sulfate ($C_{18}H_{38}N_4O_{15}S$) (Growcells), iron(III) citrate ($C_6H_5FeO_7$) (Alfa Aesar), iron(II) sulfate heptahydrate ($FeSO_4{\cdot}7H_2O$) (Alfa Aesar), 3-(2-pyridyl)-5,6-bis(4-sulfophenyl)-1,2,4-triazine disodium salt hydrate (ferrozine, $C_{20}H_{12}N_4Na_2O_6S_2$, TCI), 5-norbornene-2-carboxylic acid (Sigma-Aldrich), *N*,*N*′-diisopropylcarbodiimide (Sigma-Aldrich), 4-dimethylaminopyridine (Sigma-Aldrich), Sigmacote (Sigma-Aldrich), diethyl ether (Acros Organics), anhydrous DCM, DMSO and $CDCl_3$ (Sigma-Aldrich), DMSO-d^6 (Sigma-Aldrich), nail polish (Electron Microscopy Sciences), AlexaFluor 647, (Bioss, bs-0437R-A647), Anti-6xHistidine conjugated to SureLight APC (Columbia Biosciences, D3-1711 lot APC010-20-060), Recombinant Strepavidin Polyclonal Antibody AlexaFlour 647 Conjugated (BS-0437R-A647), BacLight Live/Dead Stain (Invitrogen), deuterium oxide (D_2O) (Sigma-Aldrich, 99.9%), Corning Dulbecco's modification of Eagle's medium (DMEM) (Fisher Scientific), fetal bovine serum (Fisher Scientific), penicillin-streptomycin solution (Fisher Scientific), Tyrpsin (Corning, 0.25% with 0.1% EDTA in Hank's buffered saline solution without calcium, magnesium and sodium bicarbonate), paraformaldehyde solution (4% in PBS, Thermo Scientific Chemicals), Triton-X-100 (Sigma-Aldrich), Blocker BSA (10X) in PBS (Thermo Scientific), rhodamine phalloidin (Invitrogen), DAPI (Sigma-Aldrich) and gelatin-methacrylate (Allevi) were used as received. All media components were autoclaved or sterilized using 0.2 µm polyethersulfone filters. Dermal Fibroblasts CC-2511 are patient derived from a 27Y female, batch 0000488388 (Lonza).

Bacteria strains and culture

Bacterial strains and plasmids are listed in Supplementary Table 1. Cultures were prepared as follows and as outlined previously[31,35]: bacterial stocks stored in 20% glycerol at −80 °C were streaked onto Luria-Bertani (LB) agar plates (for wild-type and knockout strains) or LB agar with 20 or 25 µg ml^{-1} kanamycin (for plasmid-harboring strains). Agar plates were grown overnight at 30 °C for *Shewanella* and 37 °C for *E. coli*. Single colonies were inoculated into *Shewanella* basal medium (SBM) supplemented with 100 mM HEPES, 0.05% trace mineral supplement, 0.05% casamino acids and 20 mM sodium lactate (2.85 µl of 60% w/w sodium lactate per 1 ml of culture) as the electron donor. Aerobic cultures were in 15-ml culture tubes overnight at 30 °C and 250 rpm shaking. Anaerobic cultures were using the same procedure outlined above, but in degassed growth medium, supplemented with 40 mM sodium fumarate (40 µl of a 1 M stock) in a humidified anaerobic chamber (3% H_2, balance N_2, Coy). For stationary phase conditions, inducible strains were anaerobically without inducer(s) for 4–6 h before being diluted 1:25 into inducer-containing media (from 1,000× stocks) to grow overnight. Cultures were washed three times after growth using SBM supplemented with 0.05% casamino acids (degassed for anaerobic cultures). OD_{600} was measured using a NanoDrop 2000C spectrophotometer and normalized to 10× the inoculating OD_{600} for dilution into gel mixtures (5 µl of concentrated cell culture into 45 µl of gel mixture) unless otherwise noted.

Hydrogel radical cross-linking using engineered *S. oneidensis*

$CuBr_2$ and TPMA were dissolved at 8 mM in dimethylformamide (DMF) for storage and combined into a 400 µM Cu-TPMA stock solution in DMF before reaction preparation. HEBIB (1.45 µl) was added to SBM with casamino acids (143 µl) to create a 69 mM stock solution that was diluted fivefold in SBM with casamino acids to create a 13.8 mM solution before reaction preparation. Per 50 µl hydrogel disk that was analyzed by rheology, a cross-linking reaction mixture was prepared as follows: PEG-MA was dissolved at 6.18 wt% in SBM with 0.05% casamino acids and aliquoted into an autoclaved microfuge tube (40.47 µl). Solutions of 400 µM Cu-TPMA (0.625 µl or 1.25 µl), 13.8 mM HEBIB (0.3625 µl), 60% sodium lactate (0.143 µl) and 1 M sodium fumarate (2 µl) were added to the PEG-MA solution and mixed. Per 50 µl of gel mixture, the remaining 1.4 µl was used for antibiotic and inducing molecule addition where necessary, or to compensate for varying Cu-TPMA concentration, otherwise 1.4 µl of SBM with casamino acids was added. Constituent volumes were multiplied as necessary to create a single primary stock for each experiment involving identical inducer conditions and *S. oneidensis* strains. The final concentrations in solution were 5 wt% PEG-MA, 5 or 10 µM Cu-TPMA, 100 µM HEBIB, 20 mM lactate, 40 mM fumarate and 0, 20 or 25 µg ml^{-1} kanamycin where necessary, depending on *S. oneidensis* strain. Inducer concentrations ranged from 0 to 1,000 µM depending on the condition and were diluted from 100× stock solutions. IPTG was dissolved in sterile H_2O, ATC was dissolved in a 1:1 ethanol:H_2O solution and OC6 was dissolved in DMF; all inducer stocks were stored at −20 °C. The primary gel mixture was then distributed into individual autoclaved microfuge tubes of 45 µl aliquots to which 5 µl of OD_{600}-normalized cells were added. The gel solutions were mixed and dispensed onto hydrophobically treated glass slides with a 0.5-mm silicone spacer separating the two glass layers. The gels were allowed to react at 30 °C for 2 h at inoculating OD_{600} = 0.2 (stationary phase conditions), or 16 to 24 h at inoculating OD_{600} values ranging from 0.01 to 0.05, depending on the strain (dynamic conditions). Hydrogels were removed from the slides using a razor blade and placed into 3-ml baths of 1× PBS overnight to swell to equilibrium at room temperature in the dark.

Rheological analysis

Swollen hydrogels prepared as outlined above were analyzed by oscillatory shear rheology using a TA Instruments Discovery HR-2 Rheometer utsing Trios software with an 8-mm parallel plate geometry as outlined previously[31]. Briefly, the geometry gap was lowered to an axial force at or above 0.02 N (usually between 300 and 600 µm, depending on the cross-link density and swelling ratio). Storage was measured using frequency sweeps from 0.1 to 1 Hz at a constant strain of 1%. Moduli for a single gel were quantified by averaging the linear viscoelastic region of each frequency sweep.

Plasmid construction

All bacterial strains, plasmids, genetic circuit maps and sequence information for each genetic part are detailed in Supplementary Tables 1–2 and 4. All plasmids were purchased from Addgene or assembled via Golden Gate cloning procedures using enzymes (BsaI, SapI, BsmBI) and buffers from New England Biolabs. DNA fragments used in Golden Gate cloning were generated via partial and/or whole-plasmid PCR or commercially synthesized (Integrated DNA Technologies or Twist Biosciences). Generally, 10 µl Golden Gate reactions were set up that contained 10 fmol of plasmid backbone and 40 fmol of each synthesized gene and/or PCR insert (as necessary). In a thermocycler, Golden Gate reactions were cycled 25–45 times, depending on the complexity and size of the construct: 90 s at 37 °C (for BsaI and SapI) or 42 °C (for BsmBI) followed by 3 min at 16 °C. After the cycles, reactions were incubated at 37 °C (for BsaI and SapI) or 55 °C (for BsmBI) for 5 min, 80 °C for 10 min and then held at 4 °C. Golden Gate reactions were used to directly transformed into *E. coli*, and colonies were picked

and isolated. Freshly isolated DNA was transformed into newly made electrocompotent *S. oneidensis*. To prepare electrocompetent *S. oneidensis*, 5 ml of overnight *S. oneidensis* growth in LB medium at 30 °C was washed three times with sterile 10% glycerol at room temperature and concentrated to roughly 300 µl. A approximately 1 ng of DNA was mixed with 30 µl of concentrated electrocompetent *S. oneidensis*, transferred to a 1-mm electroporation cuvette and electroporated at 1,250 V. To recover electroporated cells, 250 µl of LB warmed in a 30 °C incubator was immediately added postelectroporation and cells were incubated and/or shaken at 30 °C and 250 rpm. After 2 h of recovery, 100 µl of cell suspension was plated onto LB agar plates containing 20 or 25 µg ml^{-1} kanamycin and incubated overnight at 30 °C to obtain single colonies. Single colonies were used to inoculate LB liquid medium containing 20 or 25 µg ml^{-1} kanamycin sulfate and incubated and/or shaken overnight at 30 °C and 250 rpm. These cultures were used to generate 20–22.5% glycerol stocks that were stored at −80 °C, and to harvest assembled plasmid for Sanger sequencing (DNA Sequencing Facilities, University of Texas at Austin and Plasmidsaurus) and were confirmed on Benchling. All plasmid files are available in the Supplementary Information.

Functional verification of *mtrC* expression

Strains containing *mtrC* expression circuits were functionally validated using an in situ Fe(III) reduction–ferrozine assay as previously described[35]. In brief, strains were anaerobically pregrown for roughly 6 h in SBM containing 20 mM lactate, 40 mM fumarate and 20 or 25 µg ml^{-1} kanamycin depending on the strain. These cell suspensions were diluted 100-fold into SBM containing 20 mM lactate, 40 mM fumarate, kanamycin and appropriate inducers, then allowed to grow for roughly 18 h. Subsequently, these growths were diluted 100-fold into 96-well plates containing SBM solution with 20 mM lactate, kanamycin, 1 mg ml^{-1} ferrozine, appropriate inducers and 5 mM Fe(III) citrate, such that the final well volume was 250 µl. Fe(II) standards were also included in the plate using dissolved $FeSO_4$. The 96-well plate was sealed with a sterile and optically transparent film (PCR-SP-S, AxySeal Scientific), covered with a polystyrene plate lid (Eppendorf) with silicone grease lining the edges, removed from the anaerobic chamber and placed within a BMG LABTECH CLARIOstar plate reader with temperature control set to 30 °C. Without shaking, the absorbance at 562 nm was measured every 10 min for at least 14 h. Using the Fe(II) standards, raw kinetics data were converted to Fe(II) concentrations versus time. Fe(II) kinetics for individual replicates were background subtracted (that is, Fe(II) level at the initial time point) and fitted to an exponential Monod-type model to obtain fitted rate constants (μ)[35]:

$$\mathrm{Fe}^{\mathrm{II}}_{\mathrm{subt}} = k\,(\exp(mt) - 1) \tag{1}$$

Antibody labeling of MtrC and flow cytometry

Strains containing *mtrC* expression circuit with a streptavidin binding site on the N terminus and a polyhistidine binding site on C terminus of MtrC was pregrown overnight using standard culture conditions outlined above with the addition of 25 µg ml^{-1} kanamycin. Samples were prepared as induced, following stationary phase conditions or uninduced with or without the addition of IPTG, respectively. Cells were then pelleted and washed aerobically three times in PBS buffer (pH 7.4) at 12,000*g* for 2 min. Final resuspension in 500 µl of PBS yielded an OD_{600} of 0.4. To each suspension, 50 µl of 40 nM anti-streptavidin antibody (conjugated to AlexaFluor 647, Bioss) and 50 µl of 40 nM anti-6X-His antibody (conjugated to AlexaFluor 647, Colombia Biosciences) was added. The samples were incubated in the dark, at room temperature, while shaking for 4 h. Cells were then washed three times at 12,000*g* for 2 min to remove any unbound antibody. Final resuspension in 500 µl yielded 4×10^8 CFU per ml^{-1}. Flow cytometry was immediately performed using a BD LSRFortessa SORP Flow Cytometer. Fluorescence was measured using an APC emission–excitation laser at 635 nm, and not gated based on cell size. Data collection was performed with FACSDiva v.6.13 and data analysis was performed using FlowJo.

Quantification of fluorescence and cross-linking constructs

Strains containing *sfgfp* architectures were aerobically pregrown overnight using standard culture conditions outlined above, with the addition of 20 or 25 µg ml^{-1} kanamycin depending on the strain. Cultures were then diluted 1:25 into 96-well plates containing SBM with 0.05% casamino acids, 20 mM lactate, 40 mM fumarate, kanamycin, 5 µM Cu-TPMA, 100 µM HEBIB and varying amounts of inducer(s) (from 500× stocks). Plates were sealed with impermeable foil and placed at 30 °C for 18–24 h. Before measuring sfGFP fluorescence, protein translation was arrested by supplementing a 100 µl aliquot of cell suspension with kanamycin sulfate to a final concentration of 2 mg ml^{-1}. Subsequently, this suspension was shaken aerobically for 1 h at 30 °C to allow for sfGFP maturation. sfGFP fluorescence (488/530 nm) and cell suspension absorbance (600 nm) were measured using a BMG LABTECH CLARIOstar plate reader to yield fluorescence • absorbance^{-1} for each sample. For each sample, the background fluorescence–absorbance^{-1} from an empty vector (pCD8) control was subtracted. In addition, strains were normalized in each plate to a RNAP flux standard strain constitutively expressing *sfgfp* (pCDe1) via the Ptrc* promoter to enable REU calculations. A nonlinear fitting algorithm in GraphPad Prism v.9 was used to fit inducible gene expression to the following activating Hill function:

$$y = \min + (\max - \min)\,\frac{[I]^n}{K_{1/2}{}^n + [I]^n} \tag{2}$$

Strains containing *mtrC* architectures were analyzed similarly after rheological analysis to fit hydrogel storage modulus. Normalized hydrogel storage modulus was calculated using the average storage modulus from gels cross-linked using wild-type *S. oneidensis* harboring a representative empty vector plasmid (pCD8). Further details on modeling can be found in previous work[31,35]. Fitting parameters and 'goodness of fit' can be found in Supplementary Table 3.

CuAAC hydrogel cross-linking

$CuBr_2$ was dissolved at 8 mM in DMF for storage and combined into with THPTA or BTTAA in sterile water to form a 500 µM Cu-ligand stock solution a ratio of 1:6 Cu:ligand. Per 50 µl hydrogel disk that was analyzed by rheology, a cross-linking reaction mixture was prepared as follows: four-arm-PEG-alkyne (5 K) was dissolved at 4.62 wt% in SBM with 0.05% casamino acids and aliquoted into an autoclaved microfuge tube (18.68 µl) where it was combined with four-arm-PEG-azide (10 K) was dissolved at 8.92 wt% in SBM with 0.05% casamino acids (18.68 µl). Solutions of 500 µM Cu-THPTA (5 µl), 60% sodium lactate (0.143 µl) and 1 M sodium fumarate (1 µl) were added to the solution and mixed. Per 50 µl of gel mixture, the remaining 1.5 µl was used for antibiotic and inducing molecule addition where necessary, otherwise 1.5 µl of SBM with casamino acids was added. Constituent volumes were multiplied as necessary to create a single primary stock for each experiment involving identical inducer conditions and *S. oneidensis* strains. The final concentrations in solution were 5 wt% PEG-backbone (1.67 wt% four-arm-PEG-alkyne and 3.33 wt% four-arm-PEG-azide), 50 µM Cu-THPTA (1:6) or Cu-BTTAA (1:6), 20 mM lactate, 20 mM fumarate and 25 µg ml^{-1} kanamycin where necessary, depending on *S. oneidensis* strain. Inducer concentrations ranged from 0 to 1,000 µM depending on the condition and were diluted from 100× or 200× stock solutions. The primary gel mixture was then distributed into individual autoclaved microfuge tubes of 45 µl aliquots to which 5 µl of OD_{600}-normalized cells were added. The gel solutions were mixed and dispensed onto hydrophobically treated glass slides with a 0.5 mm silicone spacer separating the two glass layers. The gels were allowed to react at 30 °C for 12 to 16 h at inoculating OD_{600} values ranging from 0.01 to 0.05, depending on the

strain (dynamic conditions). Hydrogels were removed from the slides using a razor blade and placed into 3 ml baths of 1× PBS overnight to swell to equilibrium at room temperature.

Bacterial microscopy

Microscopy was performed using a Nikon Ti2 Eclipse inverted epifluorescence microscope. Cells assessed for viability by microscopy were cross-linked using standard conditions and the resulting gels swollen in 1× PBS at room temperature overnight. The gels were then incubated in the dark in a BacLight Live/Dead stain mix (1.5 µl ml^{-1} Syto9, 2.5 µl ml^{-1} propidium iodide in 0.85% NaCl solution) for 30 min. Stained gels were then washed by pipetting 3× in 1 ml PBS to remove unbound dye. Gels were loaded onto glass microscope slides, and a no. 1 coverslip was placed on top. The gel thickness prevented using nail polish to seal the sides, but evaporative losses were not noticeable over the course of the experiment (~30 min). Fluorescence for each stain (green for Syto9, red for propidium iodide) was measured using green fluorescent protein and Texas Red excitation–emission filter cubes on a Nikon Ti2 Eclipse using NIS-Elements AR v.5.02 software. To assess metabolic activity, gels were cross-linked with *sfgfp*-harboring strains and allowed to swell in 1× PBS. sfGFP fluorescence was assessed before induction to measure background fluorescence. Gels were then incubated in 0 µM or 1,000 µM IPTG in PBS for 24 h and monitored by fluorescence using the green fluorescent protein channel. Images were processed in FIJI v.1.0.

Functional verification of *mtrC* expression in hydrogels

ATRP hydrogels were prepared as described above using the LacI inducible MtrC strain. On removing gels from the glass slides, 10 µl of a 1 mM solution of Fe(III) citrate (in water) was added on top of each gel and allowed to incubate in a humidified incubator for 15 min. Then 10 µl of 1 mM ferrozine solution (in SBM + cas) as added on top of each gel. The reaction was allowed to take place for 10 min before a photograph was captured of the progress on top of a glass imaging box. The amount of purple was quantified using ImageJ by separating out the red channel and quantifying conversion by mean gray value.

Fibroblast culturing and seeding conditions

Dermal fibroblasts, patient derived from Lonza (NHDF-ad-Der Fibroblasts FGM-2 cryo amp, CC-2511, batch no. 0000488388), were cultured to between passage 5 and 6 in DMEM supplemented with 10% FBS and 1% penicillin-streptomycin. Media was changed every other day and cells were grown in a 37 °C incubator at 5% CO_2. To seed fibroblasts onto hydrogels, cells were washed twice with PBS, and 4 ml of warmed trypsin was added and incubated for 10 min. The trypsin was quenched in 5 ml of warmed media and centrifuged at 200*g* for 6 min. The supernatant was decanted and the cell pellet was resuspended in 1 ml of complete media. Cells were further diluted such that 250 µl seeded 15,000 cells per gel.

Hydrogels were created anaerobically and swelled overnight at room temperature in a 1% penicillin-streptomycin solution in PBS before seeding (OD_{600} inoculation of 0.02, 5 µM Cu:TPMA). To enable fibroblast adhesion, hydrogel mixtures were supplemented with 6 w/w% gelatin-methacrylate (for cell adhesion) for a final concentration of 1.34 w/v% gelatin methacrylate (GelMA). After incubating for 3 h, a further 750 µl of DMEM was added and the gels were incubated overnight.

Fibroblast staining and imaging

Media was aspirated and replaced with 500 µl of 2 v% paraformaldehyde solution in PBS. After 10 min, the solution was aspirated and replaced with the same volume of 0.2 v% Triton-X-100 with 2 v% paraformaldehyde solution. After 3 min, a 5-min wash was performed with 500 µl of PBS. A blocking buffer of 1 v% BSA was incubated at room temperature for 1 h. The blocking buffer was aspirated and replaced with 500 µl of rhodamine phalloidin solution in blocking buffer. The rhodamine solution was prepared by dissolving a vial of stain in 150 µl and diluted 1 to 100 in blocking buffer. The rhodamine phalloidin was incubated for 1 h before aspirating and replacing with 500 µl of DAPI solution for 5 min. DAPI was prepared by diluting 1 µl of stain into 500 µl of blocking buffer. The DAPI was aspirated and replaced with 1,000 µl of PBS. No staining steps included shaking or incubation at increased temperatures. The gels were imaged immediately by transferring each sample to glass slides placing the cell-side down. Between 6 and 18 images were collected for each sample imaging in the TXred (80% intensity with a 1-s exposure time), DAPI (40% intensity with a 400-ms exposure time) and in bright field. Images were quantified using the FIJI particle picker to quantify the size, overall area, circularity and roundness of each cell. Only single cells were quantified as confirmed by the presence of a single-DAPI-stained nucleus, and images were collected from at least two biological replicates and greater than 18 images. *n* values were not evaluated until merged images revealed single cells, and only single cells were evaluated.

Sample size

No statistical methods were used to predetermine sample sizes. Experiments involving bacteria were conducted in biological triplicate. Mammalian cell experiment sample size was acquired at a minimum of 25 individual cells per example[71].

Reporting summary

Further information on research design is available in the Nature Portfolio Reporting Summary linked to this article.

Data availability

The data that support the findings of this study are available within the main text and its Supplementary Information file. Experimental data supporting the findings of this study will be available through the Texas Data Repository (https://doi.org/10.18738/T8/B7GAG6). Biological materials are available upon request to B. K. Keitz. Source data are provided with this paper.

Code availability

R code for running statistical analysis will be available through the Texas Data Repository.

References

71. Yeh, Y.-C. et al. Mechanically dynamic PDMS substrates to investigate changing cell environments. *Biomaterials* **145**, 23–32 (2017).

Acknowledgements

Base plasmids for the AND and NAND circuits were generously provided by the Voigt Laboratory via Addgene (grants 49375, 49376 and 49377). This research was financially supported by the Welch Foundation (grant F-1929, B.K.K.), the National Institutes of Health under award number R35GM133640 (B.K.K.), a National Science Foundation (NSF) CAREER award (grant 1944334, B.K.K.), and the Air Force Office of Scientific Research under award number FA9550-20-1-0088 (B.K.K.). A.J.G. and G.P. were supported through NSF Graduate Research Fellowships (program award DGE-1610403). We acknowledge use of shared research facilities supported in part by the Texas Materials Institute, the Center for Dynamics and Control of Materials: an NSF MRSEC (grant DMR-1720595), and the NSF National Nanotechnology Coordinated Infrastructure (grant ECCS-1542159). A.M.R. gratefully acknowledges a Career Award at the Scientific Interface (grant 1015895) from the Burroughs Wellcome Fund. We gratefully acknowledge the use of facilities within the core microscopy lab of the Institute for Cellular and Molecular Biology, University of Texas at Austin. Nuclear

magnetic resonance spectra were collected on a Bruker Avance III HD 400 funded by the NSF (award grant CHE 1626211). Flow Cytometry was performed at the Center for Biomedical Research Support Microscopy and Imaging Facility at UT Austin (RRID grant SCR_021756). We gratefully acknowledge C. Moore for his technical advice and expertise. Schematics were created using BioRender.com, graphs were created in Prism GraphPad and Boolean logic statistics were run in R.

Author contributions

A.J.G., G.P., C.M.D. and B.K.K. conceived the project and designed research. A.J.G., G.P. and D.C. performed cross-linking experiments and rheological analysis. A.J.G., G.P., C.M.D., I.E.M.M., A.J.H., T.R.S., R.R., A.E.T. and K.C.S. performed cloning and circuit characterization by growth, fluorescence, quantitative PCR with reverse transcription and iron reduction assays. K.N.H. and G.P. designed and executed fibroblast seeding assays. T.M.F. synthesized alkyne-functionalized PEG and provided reagents. S.M.C. performed statistical analysis. A.M.R. and B.K.K. supervised research. A.J.G., G.P., C.M.D. and B.K.K. wrote the paper with input from all authors.

Competing interests

The authors declare no competing interests.

Additional information

Extended data is available for this paper at https://doi.org/10.1038/s41589-024-01628-y.

Supplementary information The online version contains supplementary material available at https://doi.org/10.1038/s41589-024-01628-y.

Correspondence and requests for materials should be addressed to Benjamin K. Keitz.

Peer review information *Nature Chemical Biology* thanks the anonymous reviewer(s) for their contribution to the peer review of this work.

Reprints and permissions information is available at www.nature.com/reprints.

https://doi.org/10.1038/s41589-024-01628-y

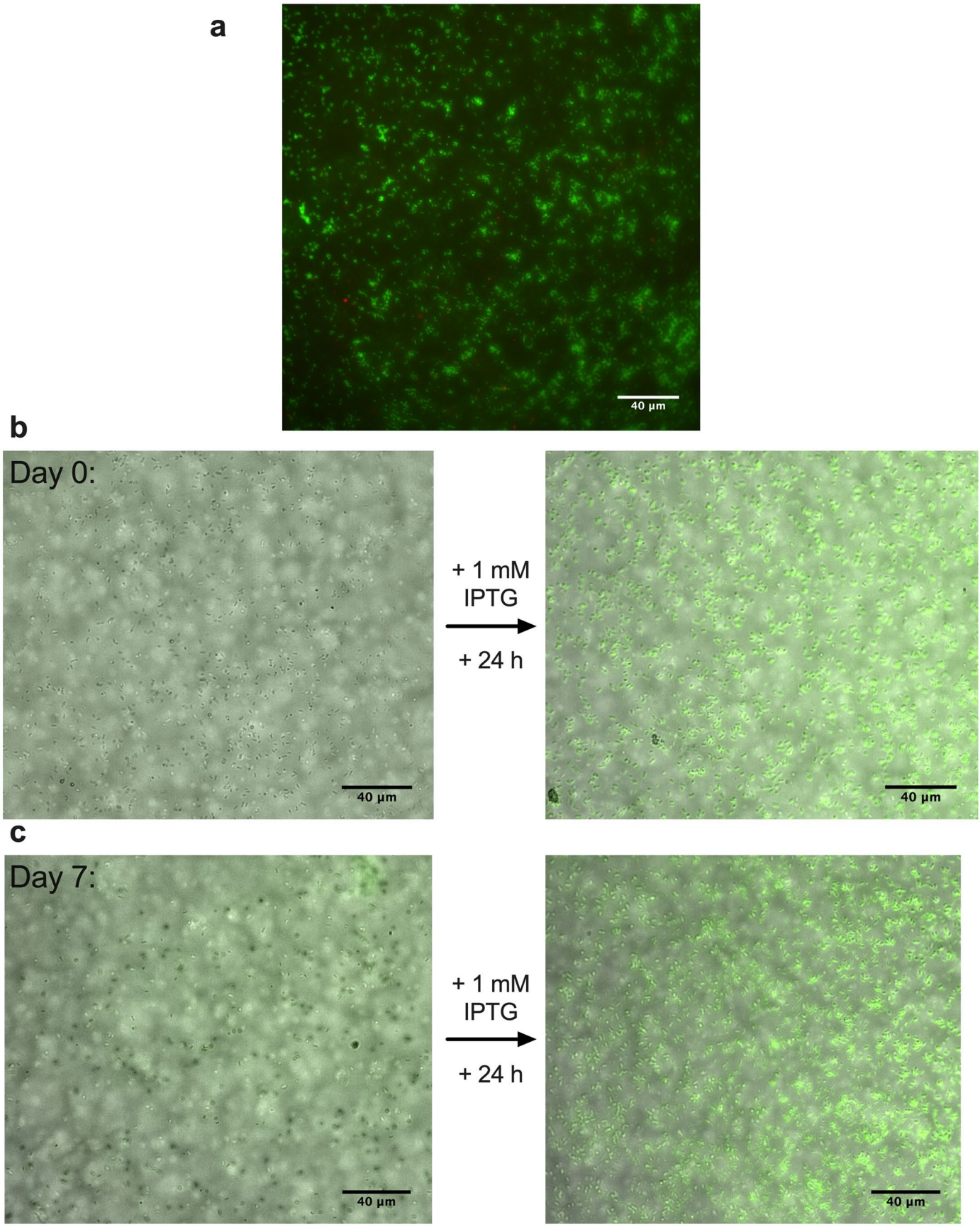

Extended Data Fig. 1 | See next page for caption.

https://doi.org/10.1038/s41589-024-01628-y

Extended Data Fig. 1 | *S. oneidensis* retains viability after cross-linking and remains metabolically active within hydrogels for at least one week. a, BacLight live/dead staining of *S. oneidensis* MR-1 after cross-linking, swelling overnight in 1x PBS, and mechanical characterization by rheology. Cells are predominantly alive (green fluorescence) as opposed to dead (red fluorescence). **b**–**c**, Overlaid fluorescence and bright-field microscopy of *S. oneidensis* MR-1 + *sfgfp* (left) encased in gels **b**, one day or **c**, one week after cross-linking and swelling, and (right) 24 h after inoculating with 1 mM IPTG to induce fluorescence. Images are representative of $n = 3$ biological replicates.

https://doi.org/10.1038/s41589-024-01628-y

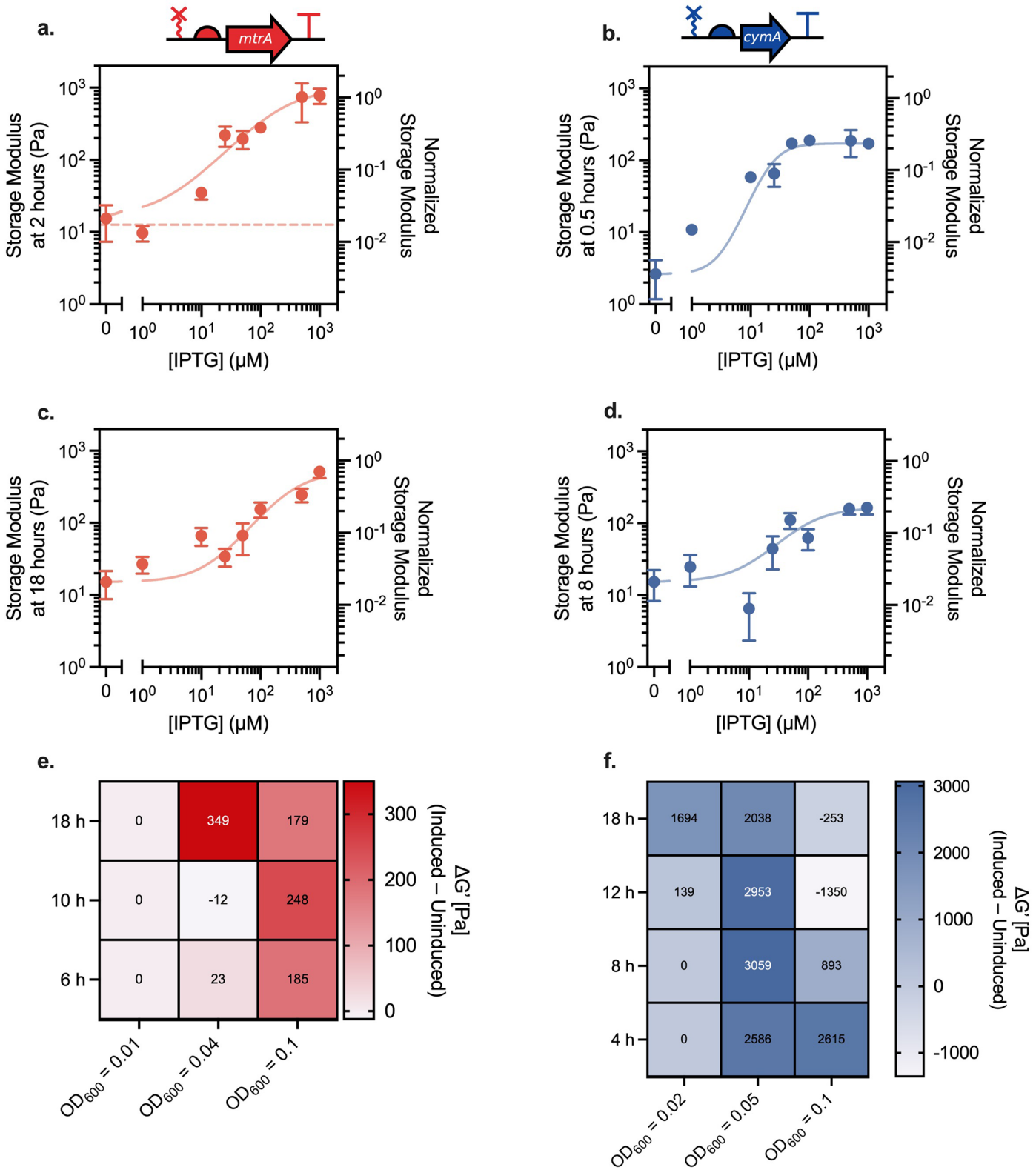

Extended Data Fig. 2 | Dynamic cross-linking couples sensing, computation, and actuation in a synthetic material. a–**d**, Cross-linking can be transcriptionally regulated using the LacI-$P_{tacsymO}$ regulator-promoter pair controlling *mtrA* (**a**) (**c**) or *cymA* (**b**), (**d**) expression under **a**-**b**, stationary phase or **c**-**d**, dynamic conditions. Data are fit to an activating gene expression model and right axis is normalized to storage modulus of gels formed using wild-type *S. oneidensis* harboring an empty vector. Dashed lines represent gel mechanics using corresponding knockout strains harboring an empty vector; if no line is shown, gels did not form. Data shown are mean ± SEM of n = 3 biological replicates. **e**-**f**, The difference between the induced and uninduced storage modulus can be controlled via both initial inoculation density and reaction time for LacI-$P_{tacsymO}$ regulator-promoter pair controlling *mtrA* (**e**) or *cymA* (**f**) (heatmap data represents n = 1).

https://doi.org/10.1038/s41589-024-01628-y

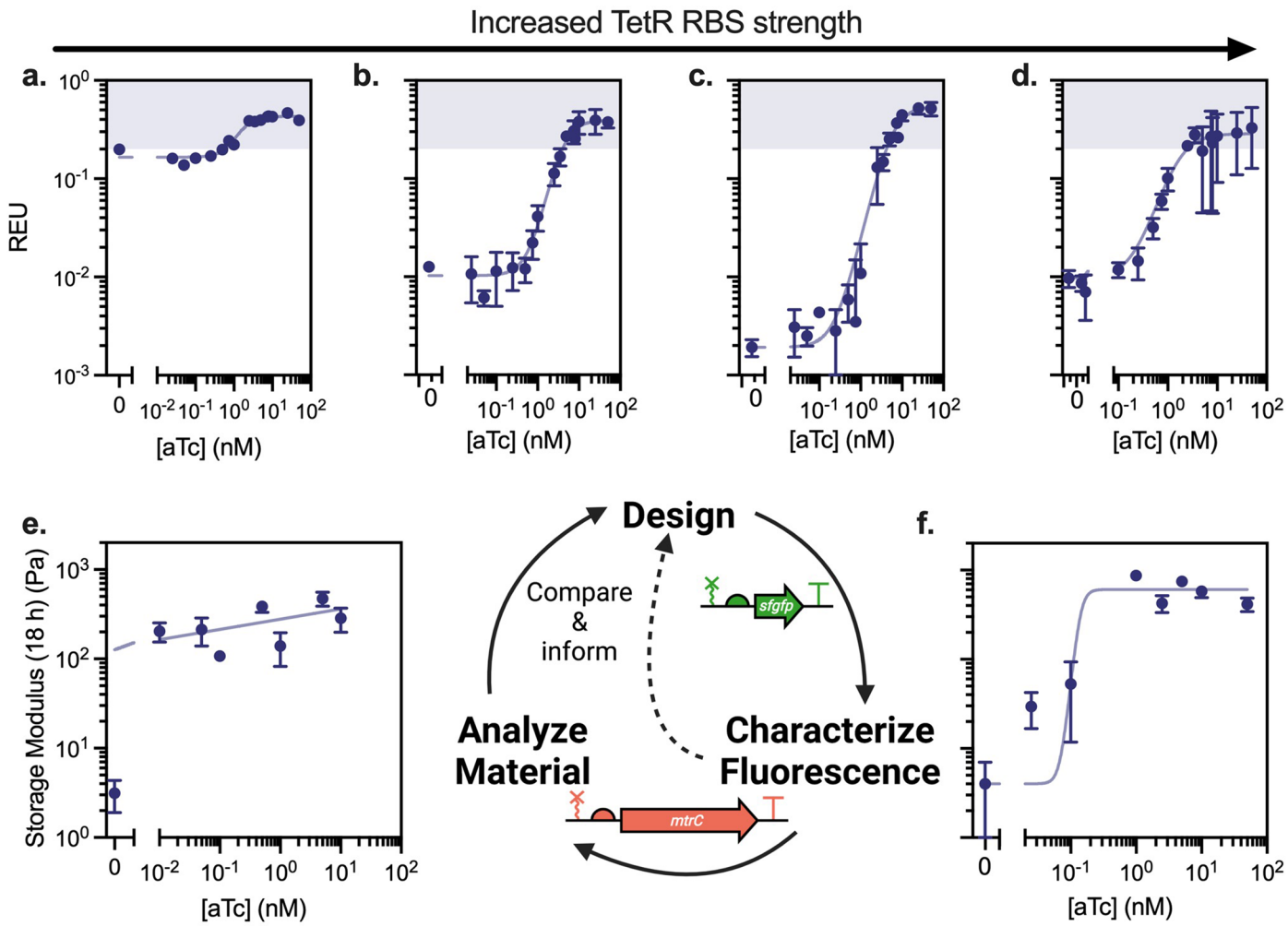

Extended Data Fig. 3 | Design, Test, Build cycle for TetR Buffer gates allows for rapid prototyping. a-d, *sfgfp response* functions for TetR-Buffer gates with varying RBS strength (800 a.u.; 2.9k a.u., 3.4k a.u.; 6.5k a.u. respectively[51]). **e**, initial material response function utilizing the same TetR-RBS strength as **a**, indicating a lack of control below REU c.a. 0.2-0.3. **f**, material response function utilizing the same TetR-RBS strength as **b**, predicting a higher dynamic range and greater control. Graphs **b**, and **f**, are reprinted from Fig. 3, but are included for clarity. Data shown are mean ± SEM of n = 3 biological replicates. Elements created with Biorender.com.

https://doi.org/10.1038/s41589-024-01628-y

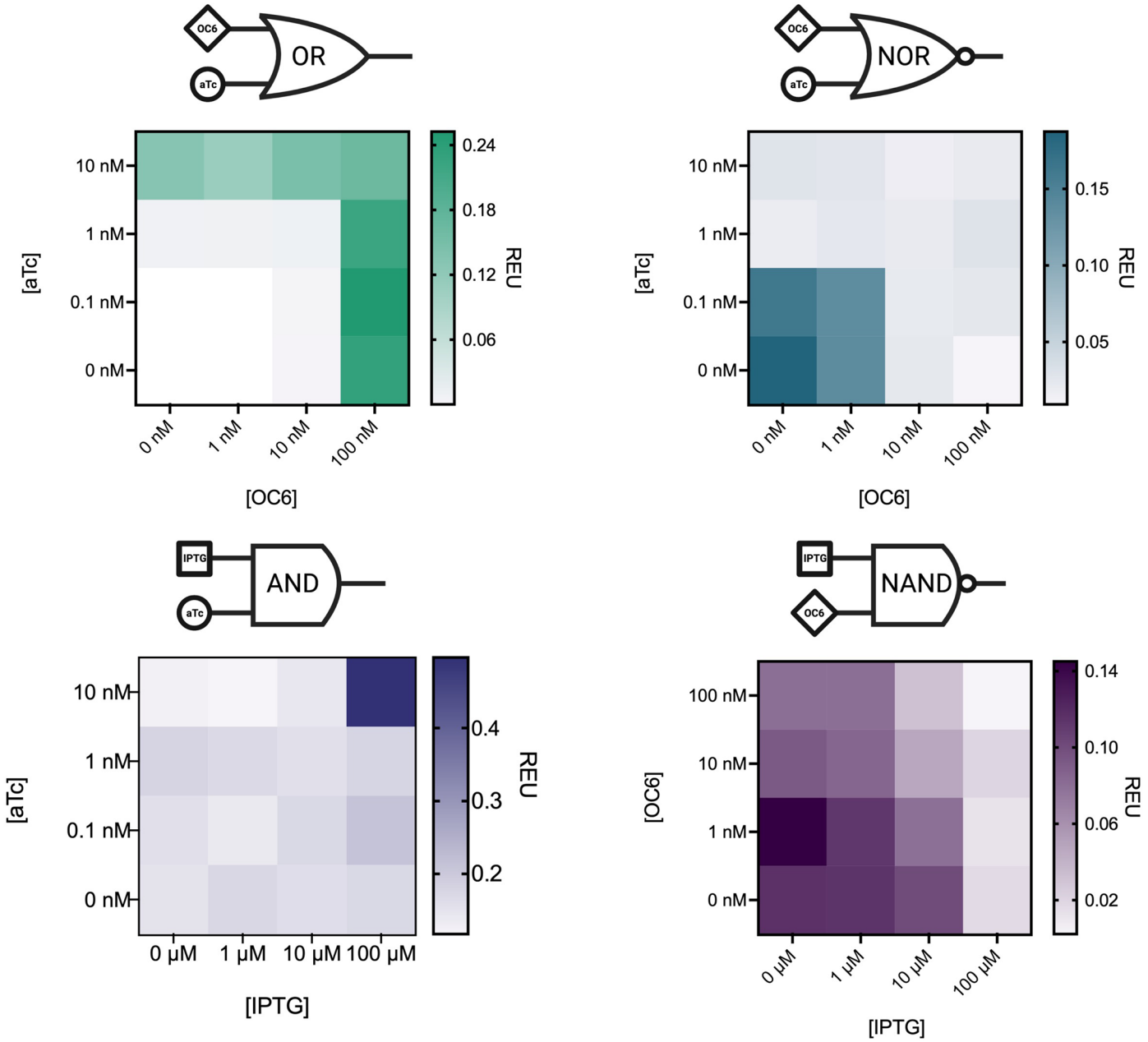

Extended Data Fig. 4 | Genetic Boolean logic enables concentration-dependent transcriptional responses in *S. oneidensis* expressing *sfgfp*. Relative Expression Units (REU) measured as a function of combinatorial inducer concentration show characteristic transcriptional regulation that follows expected truth tables for multiple genetic Boolean architectures expressing *sfgfp* (OR, NOR, NAND) or *eyfp* (AND). *S. oneidensis* MR-1 harboring each plasmid was grown overnight in aerobically prepared 96-well plates that were then sealed to emulate dynamic cross-linking conditions. Fluorescence was OD_{600}-normalized and referenced to a constitutive fluorescence plasmid to obtain REU. The expected truth tables are shown for maximum and minimum induction conditions (0, 'OFF'; 1, 'ON'). Data shown are mean of $n = 3$ biological replicates.

https://doi.org/10.1038/s41589-024-01628-y

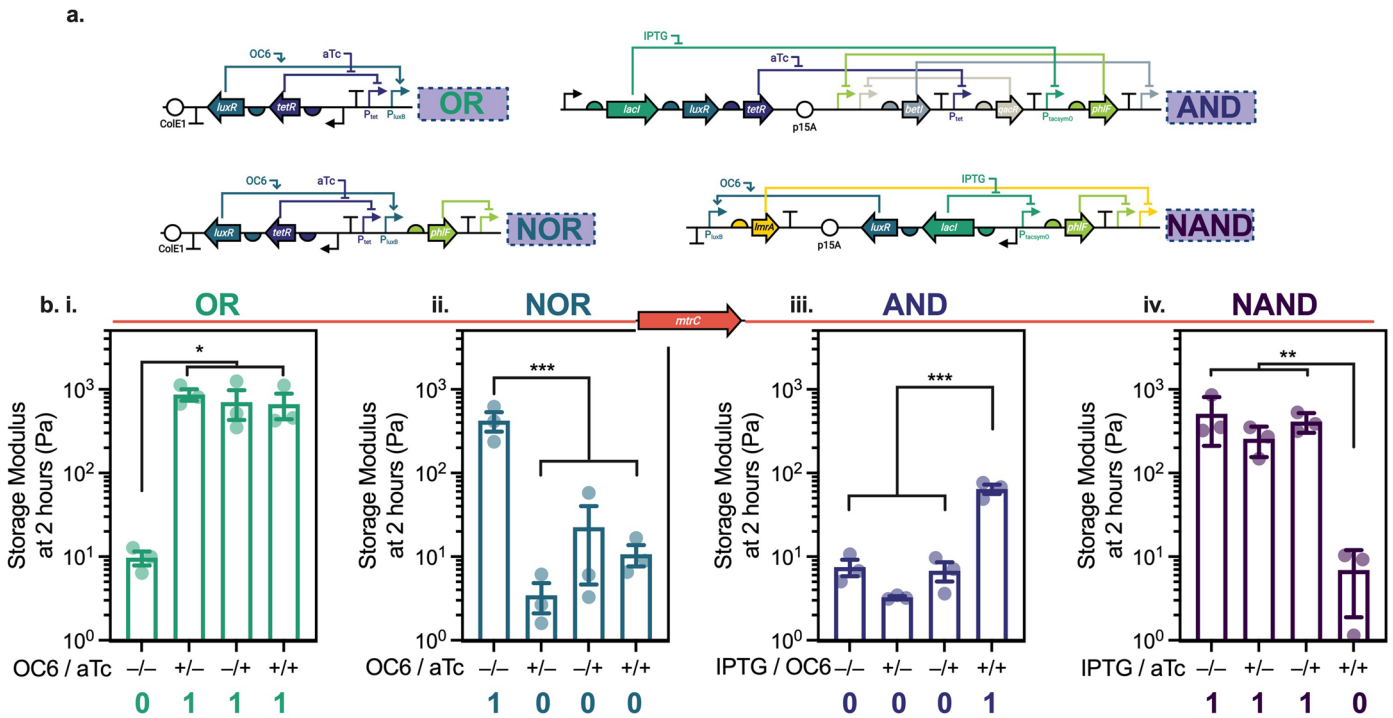

Extended Data Fig. 5 | Genetic Boolean logic enables synthetic material computation during stationary phase cross-linking. a, Storage moduli for networks cross-linked using *S. oneidensis* strains harboring transcriptional Boolean logic circuits controlling *mtrC* expression under stationary phase conditions. **b**, The logical architectures span i, OR, ii, NOR, iii, NAND, and iv, AND. In all cases, storage modulus was measured 2 h after inoculation. The expected truth tables are represented below each circuit (0, 'OFF'; 1, 'ON'). Each network appropriately responds to combinatorial inputs by increasing/decreasing storage modulus in response to *mtrC* activation/deactivation. Each plasmid architecture is shown as a cartoon above the corresponding response function, with representations as in Fig. 3. Statistics performed are the results of a general linear hypothesis test (a contrast test) between the 'OFF' and 'ON' states. Stars reference p value (* $p < 0.05$, ** $p < 0.01$, *** $p < 0.001$), R script is provided in Data Availability, and data shown are mean ± SEM of n = 3 biological replicates.

https://doi.org/10.1038/s41589-024-01628-y

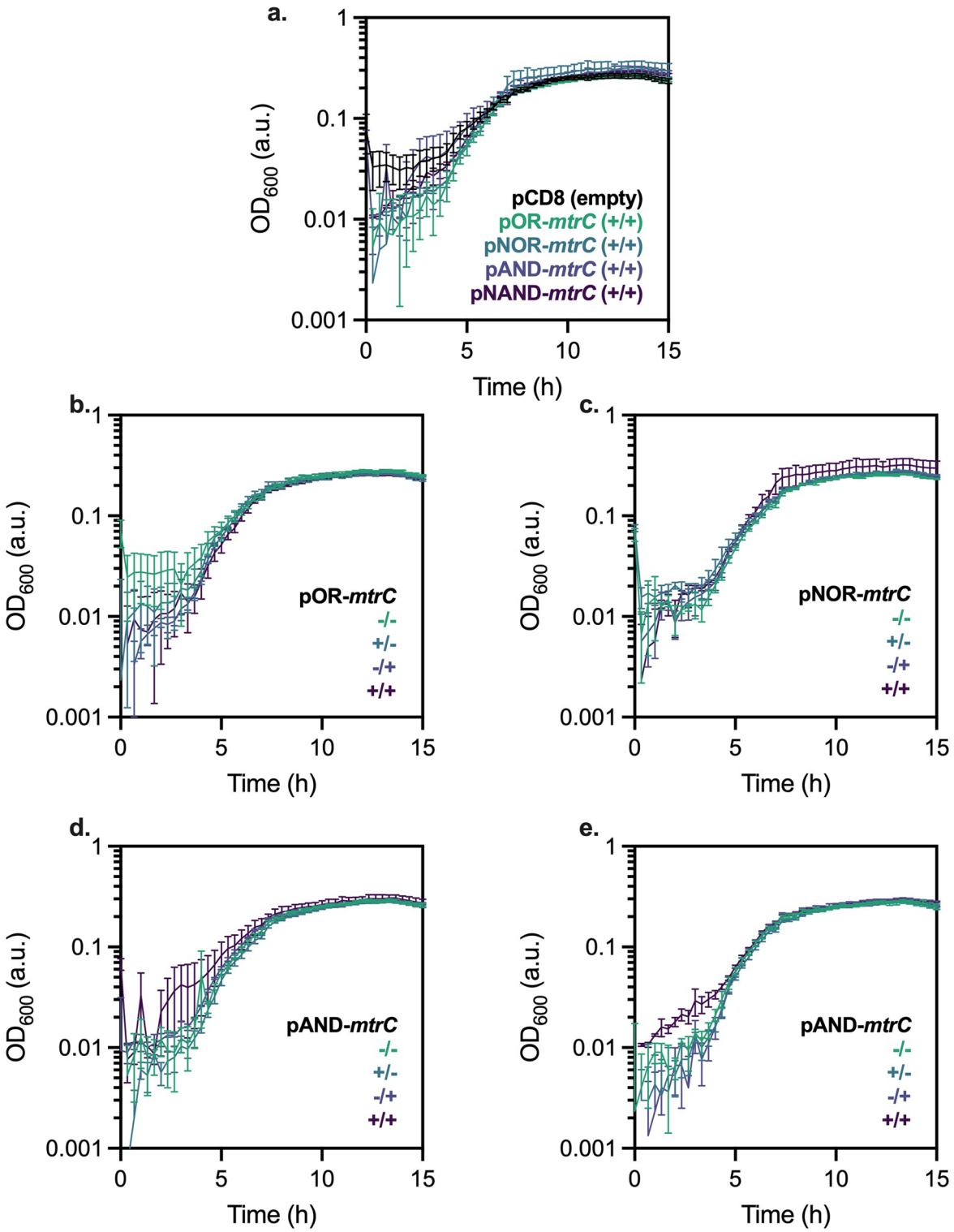

Extended Data Fig. 6 | Growth kinetics are not affected by induction in *S. oneidensis* harboring genetic Boolean logic controlling *mtrC*. OD_{600} measured *in situ* at 30 °C for *S. oneidensis* harboring each Boolean *mtrC* construct under varying inducer conditions. An induced empty vector control (pCD8) was also measured as a reference. **a**, All growth curves shown together and **b**–**e**, growth curves of individual circuits under each induction condition. In general, growth was not affected by induction. Data shown are mean ± SEM of $n = 3$ biological replicates.

https://doi.org/10.1038/s41589-024-01628-y

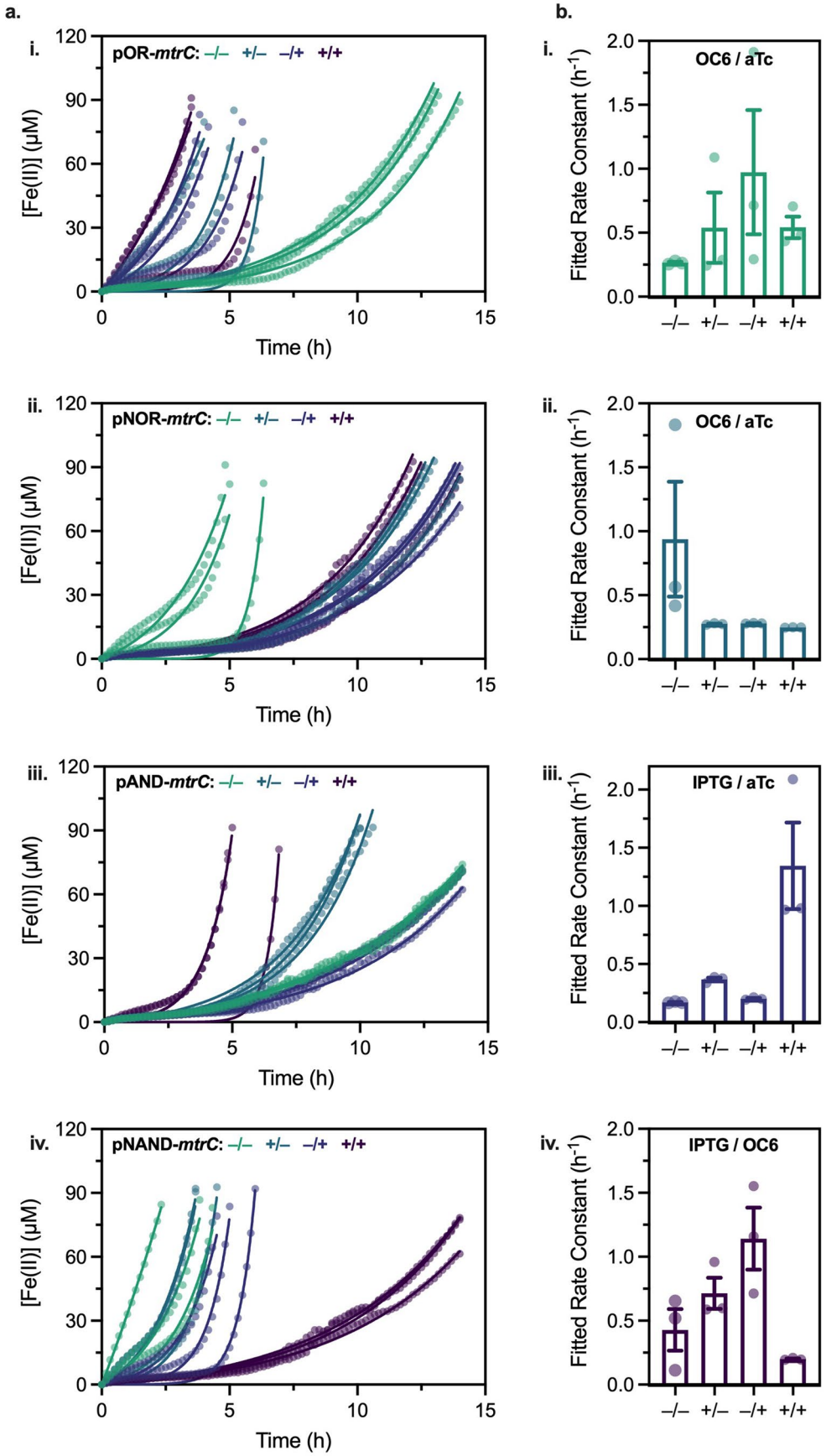

Extended Data Fig. 7 | Genetic Boolean logic enables input signal-dependent metal reduction. a, Raw *in situ* Fe(III) reduction kinetics measured using ferrozine absorbance and corresponding Monod-type fits[49]. **b**, Fitted Fe(III) reduction rate constants for corresponding curves calculated using a Monod-type model, with expected truth tables shown below (0, 'OFF'; 1, 'ON'). Gates shown are i. OR ii. NOR iii. AND iv. NAND. Data shown are mean ± SEM of $n = 3$ biological replicates.

nature portfolio

Corresponding author(s): Benjamin K. Keitz

Last updated by author(s): Mar 4, 2024

Reporting Summary

Nature Portfolio wishes to improve the reproducibility of the work that we publish. This form provides structure for consistency and transparency in reporting. For further information on Nature Portfolio policies, see our Editorial Policies and the Editorial Policy Checklist.

Statistics

For all statistical analyses, confirm that the following items are present in the figure legend, table legend, main text, or Methods section.

n/a	Confirmed
☐	☒ The exact sample size (*n*) for each experimental group/condition, given as a discrete number and unit of measurement
☐	☒ A statement on whether measurements were taken from distinct samples or whether the same sample was measured repeatedly
☐	☒ The statistical test(s) used AND whether they are one- or two-sided *Only common tests should be described solely by name; describe more complex techniques in the Methods section.*
☒	☐ A description of all covariates tested
☒	☐ A description of any assumptions or corrections, such as tests of normality and adjustment for multiple comparisons
☐	☒ A full description of the statistical parameters including central tendency (e.g. means) or other basic estimates (e.g. regression coefficient) AND variation (e.g. standard deviation) or associated estimates of uncertainty (e.g. confidence intervals)
☐	☒ For null hypothesis testing, the test statistic (e.g. *F*, *t*, *r*) with confidence intervals, effect sizes, degrees of freedom and *P* value noted *Give P values as exact values whenever suitable.*
☒	☐ For Bayesian analysis, information on the choice of priors and Markov chain Monte Carlo settings
☒	☐ For hierarchical and complex designs, identification of the appropriate level for tests and full reporting of outcomes
☐	☒ Estimates of effect sizes (e.g. Cohen's *d*, Pearson's *r*), indicating how they were calculated

Our web collection on statistics for biologists contains articles on many of the points above.

Software and code

Policy information about availability of computer code

Data collection	Rheological data were collected using a TA Instruments Discovery HR-2 and associated Trios software; sequencing & DNA design were performed using Benchling; NMR spectra were collected on a Bruker Avance 500 using MestReNova V11.1; microscopy was performed using NIS-Elements AR 5.02 and Fiji 1.0.
Data analysis	Microsoft Excel (16.8.2), GraphPad Prism 9, and R were used for data and statistical analysis.

For manuscripts utilizing custom algorithms or software that are central to the research but not yet described in published literature, software must be made available to editors and reviewers. We strongly encourage code deposition in a community repository (e.g. GitHub). See the Nature Portfolio guidelines for submitting code & software for further information.

Data

Policy information about availability of data

All manuscripts must include a data availability statement. This statement should provide the following information, where applicable:

- Accession codes, unique identifiers, or web links for publicly available datasets
- A description of any restrictions on data availability
- For clinical datasets or third party data, please ensure that the statement adheres to our policy

The data that support the findings of this study is available within the main text and its Supplementary Information file. Source data, including R code regarding statistics, is provided as Source Data files. Experimental data supporting the findings of this study will be available through the Texas Data Repository DOI: https://doi.org/10.18738/T8/B7GAG6. Biological materials are available upon request to B. K. Keitz.

Field-specific reporting

Please select the one below that is the best fit for your research. If you are not sure, read the appropriate sections before making your selection.

☒ Life sciences ☐ Behavioural & social sciences ☐ Ecological, evolutionary & environmental sciences

For a reference copy of the document with all sections, see nature.com/documents/nr-reporting-summary-flat.pdf

Life sciences study design

All studies must disclose on these points even when the disclosure is negative.

Sample size	Experiments were performed in biological triplicate (liquid cultures inoculated from three independent agar plate colonies), which was sufficient to observe significant differences in controlled gene expression behavior.
Data exclusions	No data were excluded from the analysis.
Replication	All attempts to replicate results have been successful when using freshly prepared reagents and cells. Experiments have been replicated repeatedly over the past 2 years.
Randomization	Randomization was achieved by streaking fresh agar plates of frozen bacterial stocks, and selecting single colonies from subsequent plates, yielding a random sampling of each strain tested.
Blinding	The study was not blinded as the same researchers performed grouping and measurement.

Reporting for specific materials, systems and methods

We require information from authors about some types of materials, experimental systems and methods used in many studies. Here, indicate whether each material, system or method listed is relevant to your study. If you are not sure if a list item applies to your research, read the appropriate section before selecting a response.

Materials & experimental systems

n/a	Involved in the study
☐	☒ Antibodies
☐	☒ Eukaryotic cell lines
☒	☐ Palaeontology and archaeology
☒	☐ Animals and other organisms
☒	☐ Human research participants
☒	☐ Clinical data
☒	☐ Dual use research of concern

Methods

n/a	Involved in the study
☒	☐ ChIP-seq
☒	☐ Flow cytometry
☒	☐ MRI-based neuroimaging

Antibodies

Antibodies used	Anti-6SHistidine conjugated to SureLight APC D3-1711 (Lot APC 010-20-060) ; Recombinant Strepavidin Polyclonal Antibody AlexaFlour 647 Conjugated (BS-0437R-A647)
Validation	Antibodes were validated by Columbia Biosciences and Bioss Antibodies

Eukaryotic cell lines

Policy information about cell lines

Cell line source(s)	Lonza Dermal Fibroblasts CC-2511. Patient derived from 27 year old female. Batch 0000488388 Lonza
Authentication	Cell lines were authenticated by Lonza (02/25/2020)
Mycoplasma contamination	Cell lines tested negative for mycoplasma contamination as reported by Lonza (NHDF-AD-DERFibroblasts-FGM-2)
Commonly misidentified lines (See ICLAC register)	*Name any commonly misidentified cell lines used in the study and provide a rationale for their use.*